Astronomy & Astrophysics manuscript no. AGNPSD˙OGM
March 4, 2013

© ESO 2013

arXiv:1205.4255v1 [astro-ph.HE] 18 May 2012

X-ray variability of 104 active galactic nuclei

XMM-Newton power-spectrum density profiles

O. González-Martín[1,2,3]⋆ and S. Vaughan[4]

[1] Instituto de Astrofísica de Canarias (IAC), C/Vía Láctea, s/n, E-38205 La Laguna, Spain
[2] Departamento de Astrofísica, Universidad de La Laguna (ULL), E-38205 La Laguna, Spain
[3] IESL, Foundation for Research and Technology, 711 10, Heraklion, Crete, Greece
[4] X-ray Astronomy Group, Department of Physics and Astronomy, Leicester University, Leicester LE1 7RH, UK

Received ?? 2012; accepted ??, 2012

ABSTRACT

Context. Active galactic nuclei (AGN), powered by accretion onto supermassive black holes (SMBHs), are thought to be scaled up versions of Galactic black hole X-ray binaries (BH-XRBs). In the past few years evidence of such correspondence include similarities in the broadband shape of the X-ray variability power spectra, with characteristic bend times-scales scaling with mass.

Aims. The aim of this project is to characterize the X-ray temporal properties of a sample of AGN to study the connection among different classes of AGN and their connection with BH-XRBs.

Methods. We have performed a uniform analysis of the power spectrum densities (PSDs) of 104 nearby (z< 0.4) AGN using 209 *XMM-Newton*/pn observations. These PSDs span ≃ 3 decades in temporal frequencies, ranging from minutes to days. The PSDs have been estimated in three energy bands: 0.2 − 10 (total), 0.2 − 2 (soft), and 2 − 10 keV (hard). The sample comprises 61 Type-1 AGN, 21 Type-2 AGN, 15 NLSy1, and 7 BLLACS. We have fitted each PSD to two models: (1) a single power-law model and (2) a bending power-law model.

Results. Among the entire sample, 72% show significant variability in at least one of the three bands tested. A high percentage of low-luminosity AGN do not show any significant variability (86% of LINERs). The PSD of the majority of the variable AGN was well described by a simple power-law with a mean index of $\alpha = 2.01\pm\ 0.01$. In 15 sources we found that the bending power law model was preferred with a mean slope of $\alpha = 3.08\pm\ 0.04$ and a mean bend frequency of $\langle\nu_b\rangle \simeq 2\times10^{-4}$ Hz. Only KUG 1031+398 (RE J1034+396) shows evidence for quasi-periodic oscillations. The 'fundamental plane' relating variability timescale, black hole mass, and luminosity is demonstrated using the new X-ray timing results presented here together with a compilation of the previously detected timescales from the literature.

Conclusions. Both quantitative (i.e. scaling with BH mass) and qualitative (overall PSD shapes) found in this sample of AGN are in agreement with the expectations for the SMBHs and BH-XRBs being the same phenomenon scaled-up with the size of the BH. The steep PSD slopes above the high frequency bend bear a closer resemblance to those of the 'soft/thermal dominated' BH-XRB states than other states.

Key words. Accretion, accretion disks - Galaxies:active - Galaxies:nuclei - X-ray:galaxies

1. Introduction

The dynamics of accretion around BHs should be similar for different masses, with characteristic size scales and hence timescales simply scaling with their mass (at a given accretion rate relative to the Eddington limit). Therefore, we expect to find similarities between the properties of luminous accretion flows around stellar mass BHs in X-ray binaries (BH-XRBs; $M_{BH} \sim 10$ M$_\odot$) and supermassive black holes (SMBHs) in Active Galactic Nuclei (AGN; with $M_{BH} \sim 10^6 - 10^9$ M$_\odot$). However, the details and reliability of the proposed scaling relations are currently not well understood (see Merloni et al., 2003; Körding et al., 2007; McHardy, 2010, for a review).

X-ray variability – thought to originate in the innermost regions of the accretion flow – is an important aspect of the AGN-XRB connection (e.g. Uttley et al., 2002; Markowitz et al., 2003; Vaughan et al., 2003B; McHardy et al., 2006; McHardy, 2010; Vaughan et al., 2011). Both AGN and BH-XRBs show 'red noise' power spectra (or power spectral density, PSD) that decrease steeply at high frequencies (short timescales) as a power law, $P(\nu) \sim \nu^{-\alpha}$ (where ν is temporal frequency), typically with $\alpha \approx 2$. Below some characteristic frequency ν_b the PSDs flatten, and these bend frequencies scale approximately inversely with the BH mass from BH-XRBs to AGN. However, the PSDs of BH-XRBs depend on the 'state' in which the system is observed. In the *soft state* the PSD is usually well described by a simple bending power-law, with a slope $\alpha > 2$ above some bend frequency $\nu_{\rm b}$, and a slope of $\alpha \approx 1$ extending unbroken to much lower frequencies (Cui et al., 1997). In the *hard state* the PSDs are generally more complex, with additional bends and peaks at lower frequencies, and are usually modeled as a mixture of zero-centred Lorentzian components (see e.g. Remillard & McClintock, 2006; Wilms et al., 2006). In addition there are transitional states that display a range of timing behavior. The accretion 'states' of AGN are not clearly understood (Körding et al., 2006; Fender et al., 2006) but there is some evidence to support the idea that luminous, radio-quiet AGN represent supermassive analogues of BH-XRB in the 'soft states' (Uttley et al., 2002; McHardy et al., 2004; Uttley & McHardy, 2005; Vaughan et al., 2011).

⋆ Juan de la Cierva fellow (e-mail: `omairagm@iac.es`)

One striking and common property of the X-ray variability of BH-XRBs is the prominent quasi-periodic oscillations (QPOs, see e.g. Remillard & McClintock, 2006), which are seen as strong, narrow peaks in the PSDs. Until recently there were no robust claims of QPOs in AGN (see e.g. Vaughan & Uttley, 2005). This changed when Gierliński et al. (2008) reported a QPO for the Narrow-line Seyfert 1 (NLSy1) RE J1034+396, which remains the only case to date for an AGN (see also Middleton et al., 2009; Vaughan, 2010).

The main purpose for the present paper is to characterize the PSD of a large sample of AGN including a range of AGN subclasses. With this large sample we address some outstanding problems such as: what is the most common PSD shape for AGN? how does this compare to BH-XRBs? How does the PSD vary with AGN properties (BH mass, AGN subtype or luminosity)? Are there any other strong candidate of QPO among the AGN? We have made use of the extensive *XMM-Newton* archive to obtain a sample of 104 AGN with 209 observations of at least 40 ksec. This is the largest sample of PSDs of AGN ever analyzed.

2. The sample and the data

We have selected observations of AGN from the *XMM-Newton* public archives until February 2012. Note that this should include all the sources within the 2XMMi DR3 catalogue (Watson et al., 2009). The AGN are all identified in the catalogue of Quasars and AGN by Véron-Cetty & Véron (2010)[1] with $z < 0.4$. We have selected data according to the following inclusion criteria: (1) include one or more members of the AGN sample (search radius 9 arcmin from the centre of the FOV), and (2) observation duration $T > 40$ ksec. The second criteria ensures a reasonable frequency range for the PSD estimation (the lowest observable frequency scales is $1/T$). The final sample comprises 209 observations and 104 distinct AGN.

Table 1 gives details of the sample members and relevant *XMM-Newton* observations. The optical classification (Col. 3) is taken from Véron-Cetty & Véron (2010). Three objects (NGC 4636, NGC 4736, and NGC 6251) were re-classified into the LINER class according to González-Martín et al. (2009). The sample comprises 61 Type-1 AGN (3 QSOs, 54 Seyferts, and 4 LINERs), 21 Type-2 AGN (11 Seyferts and 10 LINERs), 15 NLSy1, and 7 BLLACs. Note that we consider S1i class in the catalogue (broad Paschen lines observed in the infrared) as Type-1 Seyfert and S1h (broad polarized Balmer lines detected) as Type-2 Seyferts. The redshifts given in Col. 4 (Tab. 1) were taken from the NASA/IPAC extragalactic database (NED[2]) using the redshift-independent distance when it was available. The cosmology assumed was $H_0 = 75$ km s^{-1} Mpc^{-1}. BH masses (M_{BH}) and bolometric luminosity (L_{bol}) reported in the literature are shown in Cols. 5 and 6 together with the corresponding reference (Col. 7). We included the reverberation mapping estimate if available and the velocity dispersion estimate using the correlation reported by Tremaine et al. (2002) otherwise. The velocity dispersions are taken from HyperLeda database[3].

3. Data reduction

XMM-Newton data were processed using the SAS (v10.0.2) and the most recent calibration files available. In this paper, only the EPIC pn data (Strüder et al., 2001) were analyzed; the pn data have a higher count rate and lower pile-up distortion than the MOS data (the effect of pile-up on PSD estimation is discussed by Tomsick et al., 2004).

Time intervals of quiescent particle background were determined through an algorithm that maximizes the signal-to-noise ratio of the net source spectrum by applying different constant count rate threshold on time series of single-event, E>10 keV events, from the full field-of-view (Piconcelli et al., 2004).

The AGN sky coordinates were retrieved from NED[4] and source counts in each case were accumulated from a circular aperture of radius 40 arcsec[5]). The background events were selected from a source-free circular region on the same CCD chip as the source. We selected only single and double pixel events (i.e. `PATTERN==0-4`). Bad pixels and events too close to the edges of the CCD chip were rejected (using the standard `FLAG==0` inclusion criterion).

Source and background light curves were extracted (using EVSELECT) in 100s time bins, in three energy ranges: 0.5 – 10 keV (total band, T), 0.5 – 2 keV (soft band, S), and 2 – 10 keV (hard band, H). These were screened for high background and flaring activity (see González-Martín et al., 2011, for a detailed explanation of the procedure). High background periods at the beginning and/or end of an observation were removed. Where short periods of high background occurred in the middle of observations we excised the bad data and used the expected values derived by a linear interpolation of the neighbor data points to replace the missing data. This replacement is only done when less than 5 consecutive points need to be interpolated. For longer periods, the lightcurve is truncated selecting the largest consecutive period. Note that drop outs are less than 1% of the duration of the light-curve in all the observations presented here. Only light curves with remaining good durations longer than 40 ks were considered for further analysis. The net exposure times are listed in Col. 8 of table 1. We also extracted the EPIC-pn spectra, with response matrix and auxiliary files generated using RMFGEN and ARFGEN, respectively.

4. Data analysis

4.1. Hard band 2-10 keV luminosity estimates

The 2 – 10 keV luminosity was estimate by fitting the 2 – 10 keV spectrum using an absorbed power-law model (using XSPEC version 12.6.9q). For the Galactic absorption we used the hydrogen column density (N_H) estimates from the HI maps of Dickey & Lockman (1990). Additional absorption was also considered to account for the curvature of the spectrum of some AGN. The free parameters in the model were the intrinsic N_H, spectral index, and the power-law normalization. We did not attempt a more detailed spectral analysis, as we required only reasonable estimates of the X-ray luminosity. This method was already used by Ho et al. (2001) to estimate the luminosity in sources with low signal-to-noise data. The resulting 2 – 10 keV luminosities are given in Col. 10 of Table 1.

We have compared these luminosities with those for the same objects reported by González-Martín et al. (2009); Panessa et al. (2006); O'Neill et al. (2005, and references therein). LLAGN (i.e. Type-2 Seyferts and LINERs) show a very good agreement while Type-1 Seyferts, QSOs, and NLSy1 show the highest discrepancies, as expected due to the high long-term variability. NLSy1 show strong soft excesses interpreted as optically thick material seen in reflection (Crummy et al., 2006) or optically thin material seen in absorption (Gierliński & Done, 2004). This soft-excess shows long-term variability (see Boller et al., 1996, and references therein).

---

[1] http://heasarc.nasa.gov/W3Browse/all/veroncat. html

[2] http://nedwww.ipac.caltech.edu

[3] http://leda.univ-lyon1.fr

[4] The NASA/IPAC Extragalactic Database (NED): `http://ned.ipac.caltech.edu/`

[5] This includes approximately 90 per cent of the PSF for an on-axis source with the EPIC pn instrument.

4.2. Power spectrum estimation

The PSD gives the distribution of variability power (amplitude squared) as a function of the temporal frequency. The standard method for estimating the PSD is by calculating the periodogram (Priestley, 1981; Percival & Walden, 1993; Vaughan et al., 2003A). Fig. 1 shows the periodogram for Mrk 335. All the periodograms of the sample are shown in the electronic edition of the paper. We use the "(rms/mean)^2" normalisation throughout (see Vaughan et al., 2003A, and references therein).

The periodogram data were fitted using the maximum likelihood method discussed in Vaughan (2010, hereinafter V10) and Barret & Vaughan (2012). For a given parametric model $P(\nu;\theta)$, the best-fitting model parameters, θ, were found by maximizing the likelihood function, which in practice was done by minimizing the following fit statistic

$$S = 2\sum_{j=1}^{N/2}\left\{\frac{I_j}{P_j} + \log P_j\right\} \tag{1}$$

This is (twice) the minus log-likelihood, where I_j and P_j are the observed periodogram and the model spectral density at Fourier frequency ν_j, respectively. Confidence intervals on each model parameter were estimated by finding the set of parameter values for which $\Delta S = S(\theta) - S_{\min} \leq 1.0$, this corresponds to 68.3% intervals (this closely parallels the ΔC method discussed by Cash, 1979). See also Vaughan et al. (2005).

Following the previous work on the PSDs of AGN we used two models:

- Model A: simple power law plus constant (denoted H_0 by V10).

  $$P(\nu) = N\nu^{-\alpha} + C \tag{2}$$

  The model has three parameters: N, the power law normalization; α, the spectral index; C, an additive constant to account for Poisson noise.
- Model B: a bending power law plus constant (denoted H_1 by V10).

  $$P(\nu) = N\nu^{-1}\left(1 + \left\{\frac{\nu}{\nu_b}\right\}^{\alpha-1}\right)^{-1} + C \tag{3}$$

  The free parameters for this model are: the normalization N, the spectral index above the bend α, the bend frequency ν_b, and the constant C.

These *XMM-Newton* data are relatively insensitive to the exact low frequency index, and we assume the typical value of 1 found from long-term X-ray monitoring studies (e.g. Uttley et al., 2002; Markowitz et al., 2003; McHardy et al., 2004, 2006). The lowest frequencies available with these *XMM-Newton* data are $\sim 0.7 - 2.5 \times 10^{-5}$ Hz (set by the minimum and maximum duration of continuous observations, 40 and $\sim$ 130 ks respectively). The typical high frequency bend for a low mass Seyfert galaxy occurs at around $\nu_b \sim few 10^{-4}$ Hz, which implies only $\sim 10 - 40$ Fourier frequencies below ν_b, usually insufficient to obtain a precisely constrained power law index.

Temporally close observations of the same objects were analyzed together to better constrain the final parameters (the periodograms were fitted simultaneously with all parameters except C tried between the datasets). Note that we consider as temporally close observations those coming from the same observing run according to the first 6 digits of the ObsID. The resulting parameters are shown in tables 2 and 3.

The Likelihood Ratio Test (LRT) was used to select between the two models. The simpler model (A) is preferred in the absence of a strong preference for the more complex model (B). For reasons explained by Protassov et al. (2002) and Freeman et al. (1999) the LRT is not well calibrated when when the null values of the additional parameter of the more complex model are not well defined, as is the case here (e.g. the null value for the bend frequency in Model B is not well defined in this sense). An accurate calibration of this test using posterior predictive checks can be computationally expensive (see V10), so in this case we used the standard LRT with a $p < 0.01$ significance threshold as a crude but simple check for the presence of a bend in the PSD. The simulation results of V10 suggest that this criterion is conservative in the sence that the number of false positives is fewer than expected. Where a bend is detected (i.e. Model B selected) we parametrized the PSD amplitude at the bend frequency as $A_{psd} = \nu_b \times P(\nu_b) = N/2$ (following Papadakis, 2004), where N is the normalisation (equation 3), i.e. the peak in $\nu \times P(\nu)$ space.

The Poisson noise level, C, was usually considered a free parameter. The expected Poisson noise level was calculated assuming the standard formula (e.g. Uttley et al., 2002; Vaughan et al., 2003A) and this value was used in cases where the parameter C was poorly constrained in the periodogram fitting (these observations are indicated by an asterisk in tables 2 and 3).

As a crude but simple check for the presence of highly coherent oscillations (strictly or quasi-periodic) we identify the largest data/model outlier from each periodogram. This was then compared to the χ^2_2 distribution expected for periodogram data to give a p-value. Candidate QPOs were flagged when a $p < 0.01$ criterion was met (after correcting for the number of frequencies in the periodogram). A similar test was applied to the periodogram data after smoothing using a three-point top-hat filter, i.e. testing the running mean of each triplet of adjacent points. This test improves sensitivity to QPOs that are broader than the frequency resolution of the data. These p-values are not correctly calibrated, for reasons explained in Vaughan (2010), but such tests proved to be extremely efficient as a crude indicator of potentially interesting data.

There are two main types of bias that may effect Fourier-based power spectral analysis, 'aliasing' and 'leakage' (see Priestley, 1981; Percival & Walden, 1993; Deeter & Boynton, 1982; Uttley et al., 2002). Aliasing is negligible for the present data, which are contiguously sampled. Leakage may however cause intrinsically steep power spectra (power law indices $\alpha \gtrsim 2$) to show slopes close to $\alpha = 2$. This point is discussed further in section 5.7.

5. Results

5.1. Variability of the sample

We considered an observation variable if there was an excess above the constant value expected from the Poisson noise in the

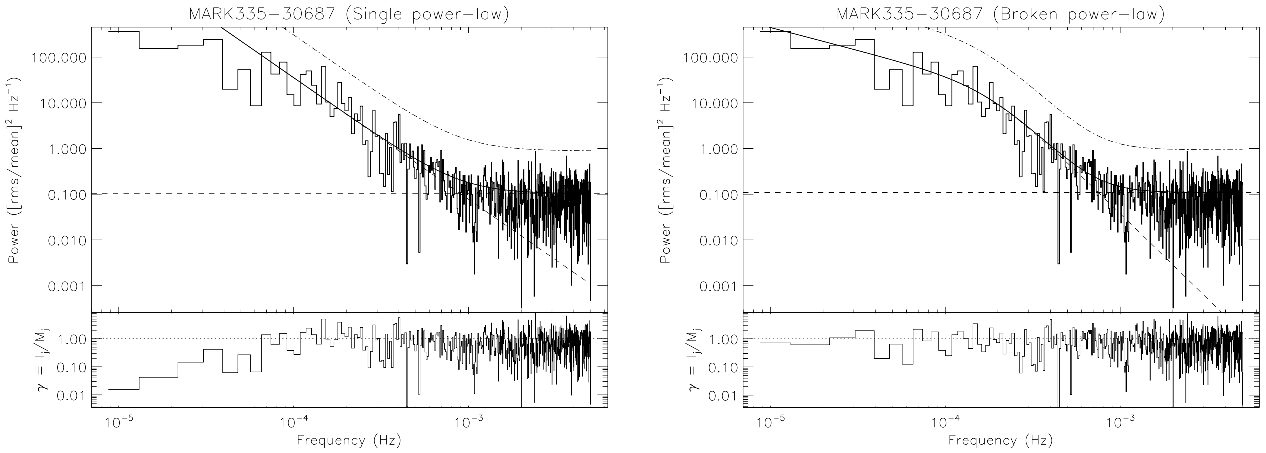

Fig. 1. PSDs fits (continuous line) to Model A (left) and Model B (right) for the Mrk 335 data (ObsID 306870101) using the broad (0.2 – 10 keV) energy band. The dashed lines shows the two components of the model: constant Poisson noise and the source PSD model (power-law, left; bending power-law, right). The dot-dashed line shows the 'global' 90% confidence limit use to flag QPO candidates. Appendix B shows the corresponding figures for the complete sample.

periodogram. We report the detection of variability in Col. 9 of Table 1 as: (T) for the total 0.5 – 10 keV, (S) for the soft 0.5 – 2 keV, and (H) for the hard 2 – 10 keV energy bands; (N) indicates no variability detected in any band.

Seventy five out of the 104 AGN (72%) showed variability in at least in one of the three bands tested. Among them, 56 showed significant variability in the total band, while three varied only in the hard band (NGC 985, 2E 0414+0057, and NGC 4258). Twenty nine of the 104 AGN (28%) did not show significant variability in any of the three bands tested. These sources are: 12 of the 14 LINERs; 2 of the 11 Type-2 Seyferts; 12 of 54 Type-1 Seyferts; 2 of the 3 QSOs; and 1 of the 7 BL Lacs. All the NLSy1s and 78% of the Type-1 Seyferts were variable, but most of LINERs are not variable. Finally, five sources were variable only in some of the observations (namely, OJ +287, NGC 2992, PG 1116+215, Mrk 279, Mrk 205, 3C 273, X Com, and RBS 1399). The lack of detected variations in these cases can be attributed to the limited quality of the data.

5.2. Model selection

Among the variable sources, we have been unable to constrain the parameters of Model A in six sources, and an additional nine have unconstrained values in a subset of the observations and/or energy bands (marked as ♣ in Table 2). This is due to the low number of bins in the PSD above the Poisson noise (e.g. see Fig. 1 of NGC 4151, ObdID = 112830201, for the total energy band in the electronic edition).

Model B is selected over Model A (using the LRT) in 17 AGN (44 observations, see Tab. 3). However, MS 22549-3712 and Mrk 586 gave very poorly constrained parameters for Model B. We consider these two sources as tentative detections of a bending PSD. Moreover, we have found a break in PKS 0558-504 far from that reported by Papadakis et al. (2010). However, our bend is more likely a bump on the PSD or a broad QPO as claimed by Papadakis et al. (2010). All the objects for which Model B was selected are Type-1 AGN but the Circinus galaxy.

5.3. QPO detection

The test for highly periodic oscillations found no candidates besides KUG 1031+398 (better known as RE J1034+396). A QPO of a $\nu_b = 2.6 \times 10^{-4}$ Hz was previously detected in this source by Gierliński et al. (2008). The apparent significance of the QPO is lower than that reported by Gierliński et al. (2008), for reasons discussed by V10.

A QPO candidate was previously reported for 3C 273 by Espaillat et al. (2008) using a wavelet technique to analyze 19 observations of 10 AGN obtained with *XMM-Newton*. For 3C 273 they used four *XMM-Newton* observations, all of them included in our analysis. We found no indication of a QPO from these data. Another case of QPO reported in the literature is the blazar PKS 2155-304. Lachowicz et al. (2009) reported a 4.6 h QPO in the 0.3 – 10 keV data (from ObsID 158961401). We have analyzed 8 observations of this source, including this one; none showed indications of a QPO. Gaur et al. (2010) analyzed all the *XMM-Newton* archival data of this source and reported a possible QPO in only one observation. This observation is included in our analysis and the hint of the QPO around 1.7×10^{-4} Hz can be seen in our PSD (see Fig. 1, in the electronic edition), consistent with their findings. However, the strength of this fluctuation above the continuum is not strong enough to suggest a QPO detection.

5.4. Slopes

The mean and standard deviation of the power law indices using Model A (for observation where Model B is not selected) was $\alpha = 2.01 \pm 0.01$ for the total energy band ($\alpha = 2.06 \pm 0.01$ and $\alpha = 1.77 \pm 0.01$ for the soft and hard bands, respectively). Fig. 2 (black filled histogram) shows the distribution of this parameter for the three energy bands[6]. The distributions are statistically indistinguishable according to the K-S test.

---

[6] Where more than one observation was available for the same object we computed the weighted mean. This was calculated only in the case of multiple distinct observations; when multiple observations occurred close in time the periodogram data were fitted simultaneously (see Section 4.2).

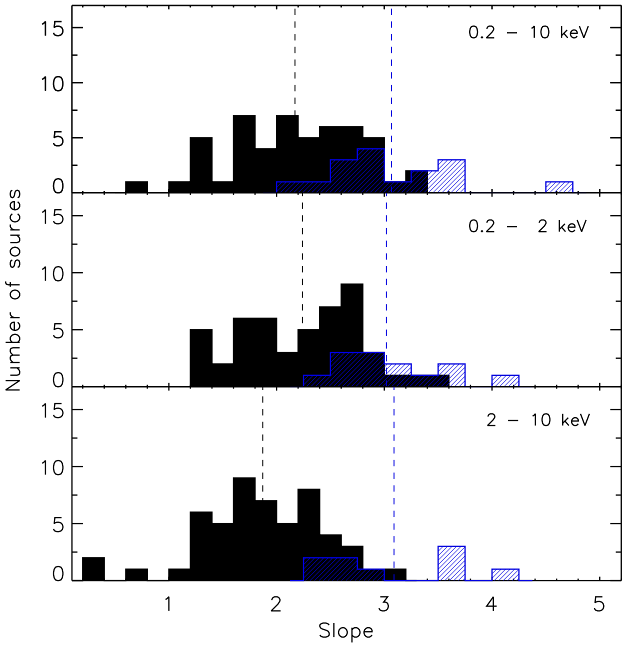

Fig. 2. Histograms of power-law slopes for Model A (black-filled histogram) and Model B (blue-dashed histogram). Top, middle, and bottom panels show the histograms for the total, soft, and hard bands, respectively. The dashed-lines show the mean value for each distribution.

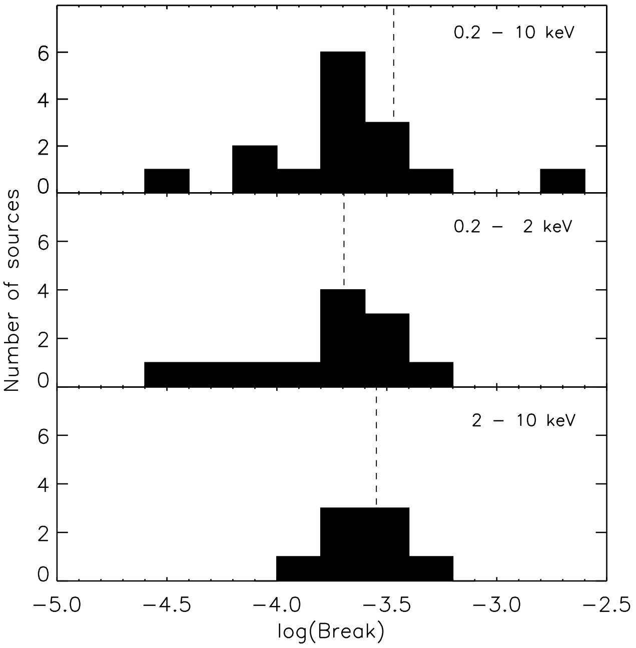

Fig. 3. Histograms of the bend frequency for Model B. Top, middle, and bottom panels show the histograms for the total, soft, and hard bands, respectively. The dashed-lines show the mean value for each distribution.

The mean value of the slope α when Model B model is preferred is $\alpha = 3.08 \pm 0.04$ for the total energy band ($\alpha = 3.03 \pm 0.01$ and $\alpha = 3.15 \pm 0.08$ for the soft and hard energy bands, respectively). These slopes are significantly steeper than those found from the Model A fit, i.e. where no PSD bend was detected. Fig. 2 (blue-dashed filled histogram) shows the distributions of slopes when Model B is preferred.

5.5. Frequency bend

We have found PSD bends for 17 AGN. Fig. 3 shows the histograms of frequency bends. Note that the weighted mean value is reported when more than one observation is available for the same object. The resulting mean values are $\log(\nu_{\rm br}) = -3.47 \pm 0.10$ for the total band (results for the soft and hard bands were almost identical).

Table 3 shows the PSD model parameters for the objects where Model B was selected. Of these, seven have not been previously reported in the literature: ESO 113-G10, Mrk 586, 1H0707-495, ESO 434-G40, Circinus, NGC 6860, and MS 22549-3712 (although Mrk 586 and MS 22549-3712 are weak detections, see section 5.2). Table 4 summarise the PSD information for the source bend detections in the present analysis together with a compilation of 17 AGN with PSD bend frequencies from the literature. We have examined the *XMM-Newton* data for all of them. This extend of the list of AGN with detected PSD bends to 24 objects (or 22 if we exclude Mrk 586 and MS 22549-3712). Appendix A gives a short description of the published bends together with a comparison with our results.

5.6. PSD bend amplitude

Papadakis (2004) found that the PSD amplitude at the bend frequency, in terms of $\nu \times P(\nu)$, was roughly constant over a sample of AGN, at $A_{psd} \sim 0.017$, based on an analysis of normalized excess variances. Table 4 (Col. 11) shows A_{psd} calculated from the estimated Model B parameters where a bend was detected. Although the mean value is $A = 0.009 \pm 0.011$, roughly consistent with the Papadakis (2004) result, this is dominated by three AGN with high A_{psd} values, namely 1H 0707-495, NGC 4051, and NGC 4395 (excluding PKS 0558-504 since it might not be a bend, see Section 5.2). These three sources are NLSy1s with low BH masses, which may indicate A_{psd} is not constant over all AGN but depends on M_{BH} and/or source type.

5.7. Leakage distortion

A fraction of the power below and above the observed frequency range can 'leak' into the observed bandpass due to the side-lobes of the Fejer kernel (see Priestley, 1981; Percival & Walden, 1993). This is the problem of spectral leakage, discussed by Deeter & Boynton (1982), Uttley et al. (2002) and Vaughan et al. (2003B). If the power spectrum is steep (e.g. $\alpha \gtrsim 2$) at or below the lowest observed frequency ($\nu_1 = 1/T$) this can lead to a significant distortion of the periodogram, as demonstrated by Uttley et al. (2002). However, the effect of leakage will be to reduce the sensitivity to bends, and QPOs, and bias the slope toward $\alpha = 2$, not to introduce spurious PSD features. Indeed, the detection of a bend to a flatter slope ($\alpha \lesssim 2$) at low frequencies is an indication that leakage cannot be significant. Some of the data sets for which the best-fitting model is a single power law (Model A) with slope $\alpha \approx 2$ are possibly be affected by leakage, for example NGC 3516 and NGC 4151 which are known to show bends to flatter slopes at frequencies lower than those covered by the *XMM-Newton* observations (Markowitz et al., 2003).

Fougere (1985) discussed methods to recover accurate power spectral indicies in the presence of strong leakge. The simplest

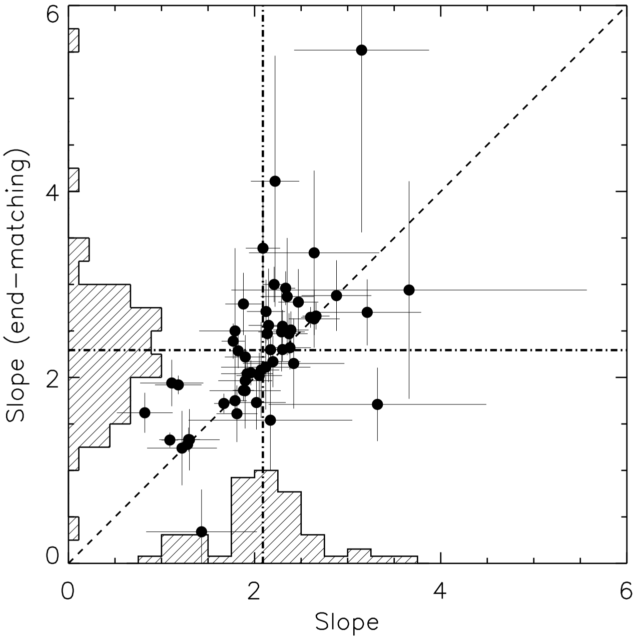

Fig. 4. Slopes obtained for Model A best-fit using the "end-matching" routine versus those obtained without using "end-matching". The dashed histograms are the normalized histograms for each distribution. The dashed line represents the one-to-one correlation and dot-dashed lines are the mean values for each distribution.

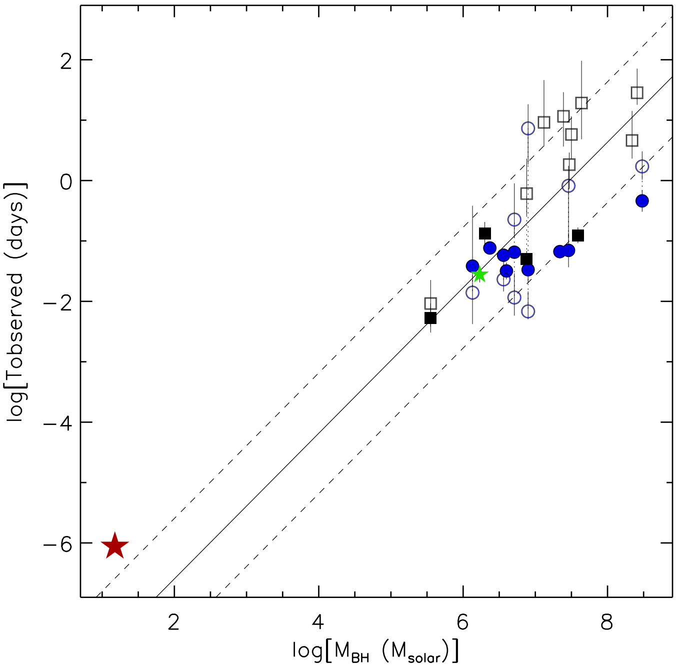

Fig. 5. Observed bend timescale versus the BH mass. The continuous line is the best-fitting following eqn. 4. The dashed lines illustrate the ±1 dex region around this model. Circles represent NLSy1s, squares represent Type-1 Seyferts, and the small green star is the Type-2 Seyfert. The open symbols are data-points reported in the literature and filled symbols are the data-points reported here. The Cygnus X-1 data are shown as a red big star. A dotted line is used to link multiple frequency bends for the same object.

method that is reasonable effective at reducing leakage bias is 'end matching', removing a linear trend from the time series such that the first and last data points have equal values. We have used this technique for those sources best fitted to Model A for the 0.2–10 keV band. We recovered Model A as the preferred fit in all cases except IGR J21277+5656 ($\log(\nu_b) = -3.84^{+0.15}_{-0.22}$, $\alpha = 2.82^{0.41}_{-0.34}$). A longer observation is needed to confirm the presence of the bend in this source. Moreover, after applying end-matching we are unable to constrain the parameters for Fairall 9. (The time series of this time series is essentially a linear trend, no short timescale variability remains after end matching.)

Fig. 4 compares the slope estimates with and without end matching. Only PKS 1547+79 shows a lower slope after the end-matching. However, the light-curve before end matching shows only a (roughly) linear trend; after end-matching no significant variability remains. The indices obtained after the end matching are on average higher than those obtained without end matching – the mean index is $< \alpha >= 2.29 \pm 0.01$ – but still significantly lower than the mean high frequency index of those sources with detected power spectral bends.

6. Discussion

6.1. Summary of results

We have presented an analysis of the high frequency power density spectra (PSD) of a sample of 104 AGN observed with *XMM-Newton*. These PSDs span up to ≈ 3 orders of magnitude in frequency, ranging from minutes to over days. Our main results can be summarized as follows:

- Variability: 72 per cent of the sample showed significant variability in at least one of the three energy bands tested. Moreover, most of LINERs in our sample do not vary (12 out of the 14 LINERs).
- PSD shape: The PSDs of the majority of the variable AGN could be described by a single power-law (i.e. Model A) with a mean slope of $\alpha \approx 2$. In 17 sources – all Type-1 Seyferts (many are NLSy1s) but the Circinus galaxy – we found a strong preference for the bending power-law model (i.e. Model B). For this subset, the slope above the bend frequency is steep, $\alpha \sim 3.0$, above a bend frequency typically around $\nu_b \sim 3.4 \times 10^{-4}$ Hz. Spectral leakage, which can bias the slope estimates in some cases, does not appear to explain discrepancy between the slopes found for Model A and B.
- QPO detection: None of the sources analyzed in our sample show a QPO, with the exception of KUG 1031+398 (RE J1034 + 396), discussed extensively in the literature.

6.2. Scaling relations

Several papers have demonstrated a strong, approximately linear correlation between the PSD bend timescale ($T_b = 1/\nu_b$) and the black hole mass (e.g. Uttley et al., 2002; Markowitz et al., 2003; Vaughan et al., 2005), as expected from simple scaling arguments (Shakura & Sunyaev, 1976; Fender et al., 2006). The simplest relation between timescale and fundamental AGN properties that we might consider is

$$\log(T_b) = A \log(M_{BH}) + C \quad (4)$$

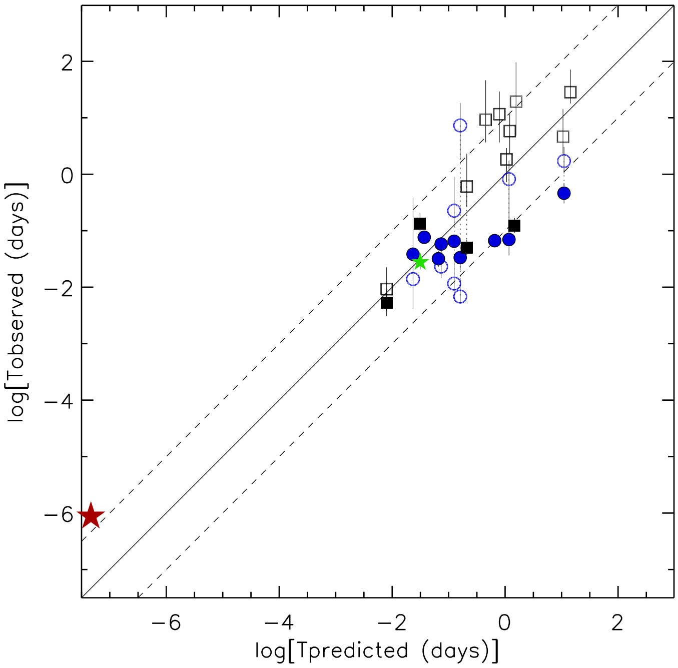

Fig. 6. Observed bend timescale against the predicted value based on the best-fitting model following eqn. 5. Symbols are the same as explained in Fig. 5.

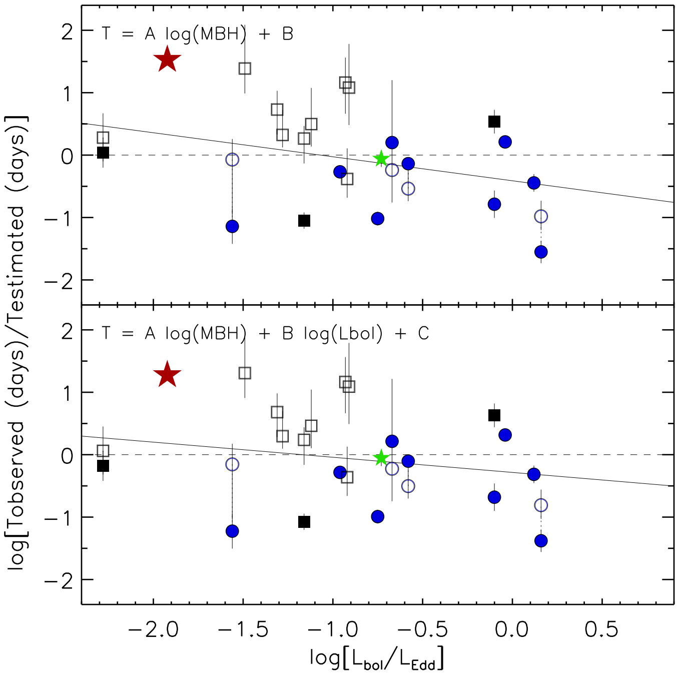

Fig. 7. Ratio between the observed and predicted T_b values against Eddington rate (L_{bol}/L_{Edd}) using eqn. 4 (top) and eqn. 5 (bottom). The continuous line shown in the top panel corresponds to the linear fit of the data. Symbols are the same as explained in Fig. 5.

where A and C are coefficients, and we expect $A \approx 1$ for a linear mass-timescale relation. McHardy et al. (2006) presented an extension of this model allowing for dependence of T_b on both M_{BH} and bolometric luminosity L_{bol}:

$$\log(T_b) = A\log(M_{BH}) + B\log(L_{bol}) + C \tag{5}$$

Table 4 gives values of $\log(\nu_b)$ for objects in which we find strong evidence for a bending power law PSD. From these we derive T_b (in units of days). This table also includes values for M_{BH} and L_{bol} taken from the literature and the values of $\log(f_b)$, M_{BH}, and L_{bol} compiled exclusively from previous literature. Together, these present the largest compilation of characteristic timescales for AGN to date. Note that the BH masses are derived by several different methods, but we have used estimates from reverberation mapping campaigns where these are available.

We fitted models following eqn. 4 and 5 to data from the 22 AGN in table 4. We have used the T_b values from our analysis when available and those from the literature otherwise, except for PKS 558-504 for which we have used the value reported in the literature[7]. The models were fitted by simple linear regression[8] (i.e. unweighted least squares) on the log transformed variables, with T_b in units of days, L_{bol} in units of 10^{44} erg s^{-1}, and M_{BH} in units of 10^6 M$_\odot$, as in McHardy et al. (2006).

Fitting equation 4 gave parameter estimates $A = 1.09 \pm 0.21$ and $C = -1.70 \pm 0.29$, leaving a sum squared error (SSE) of 11.14 (for 19 degrees of freedom, dof). The data and best-fitting regression line are shown in Fig. 5. Fitting equation 5 gave parameter estimates $A = 1.34 \pm 0.36$, $B = -0.24 \pm 0.28$, and $C = -1.88 \pm 0.36$, leaving a sum squared error (SSE) of 10.69 (for 18 dof). The parameter governing the luminosity dependence, B, is consistent with zero (p = 0.38 for 18 dof). Fig. 6 compares the bend timescale predicted by this relation (based on the observed M_{BH} and L_{bol}) to the observed T_b values (compare with Fig. 2 of McHardy et al., 2006). Fig. 7 shows the residuals (as a ratio of observed to model T_b) against L_{bol}/L_{Edd} for the two different models.

In order to test the reliability of these parameters we have used the 'bootstrap' method (Efron & Tibshirani , 1993). We generated $N = 10^4$ simulated datasets, each comprising 22 'observations' (of T_b, M_{BH}, L_{bol}) generated by drawing an AGN at random (with replacement) from the real data. This provides a simple alternative assessment of the parameter confidence intervals. The 68.3 per cent confidence intervals on the parameters are: $A = [1.02, 1.66]$, $B = [-0.52, -0.046]$ and $C = [-2.12, -1.65]$. The boostrap confidence intervals are slightly narrower than the standard regression intervals.

In order to test how well these scaling relations work over the full range of black hole masses we also show representatives values for the BH-XRB Cygnus X-1 (red star in the figures)[9]. The Cygnus X-1 points were not included in the fitting, yet are clearly consistent with an extrapolation to much lower M_{BH}, strongly supporting the reliability of such relations over the full range of M_{BH}. Indeed, fitting the two models including the Cygnus X-1 data resulted in parameter estimates consistent with those given above.

---

[7] Our bend in PKS 558-504 could the result of a bump (or broad QPO) already reported by Papadakis et al. (2010).

[8] There are several reasons for not weighting the data according to the uncertainties on T_b. Firstly, the high frequency bend in X-ray binaries is not stationary but varies in frequency by a factor of ~few, it is therefore plausible that the estimates of T_b may not represent the 'true' long-run average values if AGN power spectral are similarly non-stationary on very long timescales. Secondly, the M_{BH} and L_{bol} estimates are also subject to significant statistical and systematic errors that are difficult to quantify. These represent additional sources of variance in the data not accounted for by the confidence limits on T_b.

[9] We used the black hole mass of $M_{BH} = 15 \pm 1$M$_\odot$ recently presented by Orosz et al. (2011). For the bolometric luminosity and characteristic time scale we took the average of several estimates of the PSD bend frequency from Axelsson et al. (2006) and bolometric flux from Wilms et al. (2006) (using the data from their Model 5, Table 1 –

The main difference compared with the results obtained by McHardy et al. (2006) is a weak dependence of T_b on L_{bol} in the present analysis. This remains the case when the fitting is repeated with or without the Cygnus X-1 data (B = −0.27 ± 0.27), using a lower mass estimate for NGC 4395[10], or using a weighted least squares regression (i.e. making use of the confidence intervals on T_b). However, if we use smaller black-hole masses for NGC 4395 ((log($M_{\rm BH}$) = 4.5, see Vaughan et al., 2005; Uttley & McHardy, 2005) and NGC 5506 (log($M_{\rm BH}$) = 6.5, see McHardy et al., 2006), and NGC 6860 is removed[11], the dependence with the L_{bol} found by McHardy et al. (2006) is recovered (B = −0.70 ± 0.30, p = 0.01). Thus, this weak dependence on L_{bol} could be due to either the fact that our sample is more complete sample (more objects and new estimates from the old bends) or due to uncertainties on the BH mass and/or $L_{\rm bol}$ estimates. A bigger sample with better estimates on the BH mass and $L_{\rm bol}$ is need to check the dependence on $L_{\rm bol}$.

6.2.1. BLR versus variability

McHardy et al. (2006) also presented strong correlation between T_b and the width of the (permitted) optical lines, V, specifically Hβ. We have compiled optical line widths for the objects in Tables 3 and 4 based on the available literature. For most sources we have used as V the full width at half maximum (FWHM) of the Hβ line, the exceptions are NGC 5506 and ESO 434-G40, which are both heavily obscured and for which we have used the FWHM of the Paβ line. Fig. 8 shows the resulting timescale-FWHM relation. The linear correlation coefficient is $r = 0.692$ (highly significant; $p = 5.0 \times 10^{-4}$). Simple linear regression of $\log(T_b)$ on $\log(V)$ was used to fit a relation of the form

$$\log(T_b) = D\log(V) + E. \quad (6)$$

The best-fitting parameter values were $D = 2.9 \pm 0.7$ and $E = -10.2 \pm 2.3$, leaving a sum squared error (SSE) of 13.47 (for 19 degrees of freedom, dof). This relation is again slightly flatter than the $D = 4.2$ found by McHardy et al. (2006). The 68.3 per cent confidence intervals on these parameters calculated by the bootstrap method are $D = [2.2, 3.5]$ and $E = [-12.3, -7.9]$.

6.3. PSD shapes

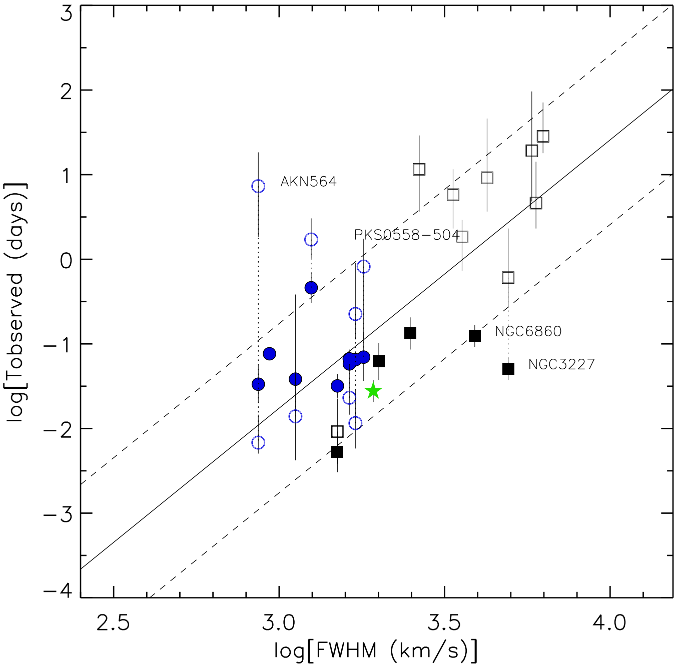

Fig. 8. Observed characteristic timescale versus the FWHM of H$_\beta$ expressed in km s^{-1}. Symbols are the same as explained in Fig. 5.

For the ten objects with well-constrained Model B parameters, the high frequency slope is steep ($\alpha \approx 3$). Such steep high frequency PSDs have been reported in the literature (e.g. Mrk 335 and Mrk 766 by Arévalo et al., 2008; Vaughan & Fabian, 2003, respectively, see our Table 4 for details), but with little explicit discussion of this point.

There seems to be no fundamental physical requirement for the PSD slope to be steeper than $\alpha = 2$ at high frequencies (see footnote 7 of Vaughan et al., 2011). Indeed, $\alpha \approx 2$ seems to be the norm for BH-XRBs in ‘hard’ states in the ∼ 5−50 Hz regime, above which there may be further steeping (Nowak et al., 1999; Revnivtsev et al., 2000). The ‘soft’ states may show steeper PSDs (Revnivtsev et al., 2000; McHardy et al., 2004), and so the steep high frequency PSDs observed from these AGN may support the argument that AGN are supermassive analogues of soft state BH-XRBs. There are alternative explanations that must be considered, however. These include the fact that the AGN PSDs presented here are based on *XMM-Newton* data with a relatively soft X-ray response, while the BH-XRB results are based on observations at harder X-rays with *RXTE*, and therefore the known energy dependence of the high frequency slope (Nowak et al., 1999; Vaughan et al., 2003B; McHardy et al., 2004) may explain the apparently steeper slopes in AGN. (We have relatively little information about the PSDs of BH-XRBs at ∼ 1 keV. See Uttley et al. 2011 for a rare example based on a bright ‘hard’ state observation.) Another possibility is that the steeper slopes are the result of a selection effect and are not representative of the larger population of bright AGN. The PSD bend is easier to detect when the high frequency slope is steep, and when the bend is at relatively low frequency. We cannot exclude the possibility that only a subset of AGN show such steep slopes but these are the ones for which the PSD bend, and hence high frequency slope, is easiest to constrain.

The majority of the sample did not show evidence of a bend (i.e. insufficient evidence to select Model B over Model A in a LRT). The mean value of the PSD index for these objects was $\alpha \approx 2$. The simplest interpretation is that these generally more

---

see McHardy et al. (2006) for justification of this choice of model). The observations were chosen to be those with simultaneous bend frequency and bolometric flux estimates. The luminosity L_{bol} was derived assuming a distance of D = 1.86 ± 0.12 kpc (Reid et al., 2011). The final bolometric luminosity and frequency bend are $L_{bol} = 2.26 \pm 0.73 \times 10^{37}$ erg s^{-1} and $\nu_b = 13.2 \pm 6.0$ Hz, respectively.

[10] NGC 4395 is the object in our sample with the most ‘leverage’ on the regression model. It could have a lower black hole mass as discussed by Vaughan et al. 2005 and Uttley & McHardy 2005 than the reverberation mapping mass of Peterson et al. (2005).

[11] We tried to remove NGC 6860 because it is one of the drop-outs in our correlation.

massive objects have lower ν_b, and hence we see only the high frequency part of the PSD. This slope is $\alpha \approx 2.3$ when the leakage distortion is reduced using end matching, but this remains flatter than the high frequency slope for objects that do show evidence for a PSD bend. It remains possible that a more rigorous method to account for the leakage bias (e.g. the methodology described by Uttley et al., 2002) could recover steeper slopes. But this could also result from a selection effect. If AGN show a wide range of high frequency PSD slopes, e.g. $\alpha \sim 2-4$ above the bend frequency, then those with flatter slopes will be more difficult to detect, as the change in slope (from the low frequency index of 1) is less pronounced.

In order to study whether we detect all the expected bends, we have computed the predicted characteristic time scale T_b for sample members with M_{BH} estimates (70 out of the 104), assuming bolometric luminosity of $L_{bol} = 30 \times L_{2-10}$ (estimated as explained in Section 4.1). The PSD bend timescales is predicted to be within the observed frequency range for only 17 sources. Of these we do indeed detect bends in 13. The exceptions are 1H 419-577, NGC 4593, IRAS 13224-3809, and NGC 7314. However, note that if we use the relation found by McHardy et al. (2006) IRAS 13224-3809 and NGC 7314 are not expected to show a bend in our frequency range. For the rest of the sample members the predicted T_b value places it outside of the observed PSD bandpass. Moreover, all the non-variable sources have an expected bend well above the range analyzed here.

6.4. Lack of QPOs

We find no strong evidence for highly coherent oscillations (QPOs) beyond the well known example of KUG 1031+398. Some authors have pointed to the extremely soft spectrum of this source as an explanation of why this source appears to be unique in showing a QPO. In fact, even for this source the QPO appears to be transient (Middleton et al., 2009, 2011). Less coherent oscillations, i.e. QPOs with a broader features in the PSD, are common to BH-XRBs, especially in harder spectral states, but are difficult to detect in the majority of the currently available data, as discussed by Vaughan & Uttley (2005) and Vaughan et al. (2011).

Acknowledgements. This research has made use of the NASA Astrophysics Data System Bibliographic Services, and the NASA/IPAC Extragalactic Data base (NED) which is operated by the Jet Propulsion Laboratory, California Institute of Technology, under contract with the National Aeronautics and Space Administration. This paper is based on observations obtained with *XMM-Newton*, an ESA science mission with instruments and contributions directly funded by ESA Member States and the USA (NASA). OGM acknoledges to the C5D00070-2006 grant of the MICINN for the finantial support. OGM thanks Dr. Iossif Papadakis for his help understanding variability processes in AGN and the interpretation of the results of the present study.

References

Arévalo, P., McHardy, I. M., & Summons, D. P. 2008, MNRAS, 388, 211
Arévalo, P., Uttley, P., Lira, P., Breedt, E., McHardy, I. M., & Churazov, E. 2009, MNRAS, 397, 2004
Axelsson, M., Borgonovo, L., & Larsson, S. 2006, A&A, 452, 975
Barret, D., Vaughan, S., 2012, ApJ, in press ((arXiv:1112.0535)
Beckmann, V., Engels, D., Bade, N., & Wucknitz, O. 2003, A&A, 401, 927
Beckmann, V., Courvoisier, T. J.-L., Gehrels, N., et al. 2008, A&A, 492, 93
Cash, W. 1979, ApJ, 228, 939
Collier, S., et al. 2001, ApJ, 561, 146
Crummy, J., Fabian, A. C., Gallo, L., & Ross, R. R. 2006, MNRAS, 365, 1067
Cui, W., Zhang, S. N., Focke, W., & Swank, J. H. 1997, ApJ, 484, 383
Belloni, T. M. 2010, Lecture Notes in Physics, Berlin Springer Verlag, 794, 53
Boller, T., Brandt, W. N., & Fink, H. 1996, A&A, 305, 53
Boroson, T. A. 2002, ApJ, 565, 78
Botte, V., Ciroi, S., di Mille, F., Rafanelli, P., & Romano, A. 2005, MNRAS, 356, 789
Deeter, J. E., & Boynton, P. E. 1982, ApJ, 261, 337
Denney, K. D., Peterson, B. M., Pogge, R. W., et al. 2009, ApJ, 704, L80
Dickey, J. M., & Lockman, F. J. 1990, ARA&A, 28, 215
Done, C., & Gierliński, M. 2005, MNRAS, 364, 208
Edelson, R., & Nandra, K. 1999, ApJ, 514, 682
Efron B. & Tibshirani R. J., 1993, *An introduction to the bootstrap*, Chapman & Hall (New York)
Eracleous, M., Hwang, J. A., & Flohic, H. M. L. G. 2010, ApJS, 187, 135
Espaillat, C., Bregman, J., Hughes, P., & Lloyd-Davies, E. 2008, ApJ, 679, 182
Fender R. P., Körding E., Belloni T., Uttley P., McHardy I., Tzioumis T., 2006, in Belloni T., ed., *Proc. Science: SISSA, VI Microquasar Workshop: Microquasars and Beyond*, preprint (arXiv:0706.3838)
Fougere, P. F. 1985, J. Geophys. Res., 90, 4355
Freeman, P. E., Graziani, C., Lamb, D. Q., Loredo, T. J., Fenimore, E. E., Murakami, T., & Yoshida, A. 1999, ApJ, 524, 753
Gaur, H., Gupta, A. C., Lachowicz, P., & Wiita, P. J. 2010, ApJ, 718, 279
Gierliński, M., & Done, C. 2004, MNRAS, 349, L7
Gierliński, M., Middleton, M., Ward, M., & Done, C. 2008, Nature, 455, 369
Gliozzi, M., Titarchuk, L., Satyapal, S., Price, D., & Jang, I. 2011, ApJ, 735, 16
Gliozzi, M., Papadakis, I. E., Grupe, D., et al. 2010, ApJ, 717, 1243
González-Martín, O., Masegosa, J., Márquez, I., Guainazzi, M., & Jiménez-Bailón, E. 2009, A&A, 506, 1107
González-Martín, O., Papadakis, I., Reig, P., & Zezas, A. 2011, A&A, 526, A132
Green, A. R., McHardy, I. M., & Lehto, H. J. 1993, MNRAS, 265, 664
Greenhill, L. J., Booth, R. S., Ellingsen, S. P., et al. 2003, ApJ, 590, 162
Grier, C. J., Peterson, B. M., Pogge, R. W., et al. 2012, ApJ, 744, L4
Gu, Q.-S., Huang, J.-S., Wilson, G., & Fazio, G. G. 2007, ApJ, 671, L105
Gültekin, K., Cackett, E. M., Miller, J. M., Di Matteo, T., Markoff, S., & Richstone, D. O. 2009, ApJ, 706, 404
Hao, L., Strauss, M. A., Fan, X., et al. 2005, AJ, 129, 1795
Ho, L. C., et al. 2001, ApJ, 549, L51
Kelly, B. C., Sobolewska, M., Siemiginowska, A., 2011, ApJ, 730, 52
Körding, E. G., Jester, S., Fender, R., 2006, MNRAS, 372, 1366
Körding, E. G., Migliari, S., Fender, R., Belloni, T., Knigge, C., & McHardy, I. 2007, MNRAS, 380, 301
Lachowicz, P., Gupta, A. C., Gaur, H., & Wiita, P. J. 2009, A&A, 506, L17
Lawrence, A., Watson, M. G., Pounds, K. A., & Elvis, M. 1987, Nature, 325, 694
Leighly, K. M. 1999, ApJS, 125, 297
Markowitz, A. 2010, ApJ, 724, 26
Markowitz, A. 2009, ApJ, 698, 1740
Markowitz, A., Papadakis, I., Arévalo, P., et al. 2007, ApJ, 656, 116
Markowitz, A. 2005, ApJ, 635, 180
Markowitz, A., et al. 2003, ApJ, 593, 96
McHardy, I., & Czerny, B. 1987, Nature, 325, 696
McHardy, I. 1988, Mem. Soc. Astron. Italiana, 59, 239
McHardy, I. M., Papadakis, I. E., Uttley, P., Page, M. J., & Mason, K. O. 2004, MNRAS, 348, 783
McHardy, I. M., Gunn, K. F., Uttley, P., & Goad, M. R. 2005, MNRAS, 359, 1469
McHardy, I. M., Koerding, E., Knigge, C., Uttley, P., & Fender, R. P. 2006, Nature, 444, 730
McHardy, I. M., Arévalo, P., Uttley, P., Papadakis, I. E., Summons, D. P., Brinkmann, W., & Page, M. J. 2007, MNRAS, 382, 985
McHardy, I. 2010, Lecture Notes in Physics, Berlin Springer Verlag, 794, 203
Mehdipour, M., Branduardi-Raymont, G., & Page, M. J. 2012, arXiv:1204.2826
Merloni, A., Heinz, S., & di Matteo, T. 2003, MNRAS, 345, 1057
Meyer-Hofmeister, E., & Meyer, F. 2011, A&A, 527, A127
Middleton, M., Done, C., Ward, M., Gierliński, M., & Schurch, N. 2009, MNRAS, 394, 250
Middleton, M., Uttley, P., Done, C., 2011, MNRAS, 417, 250
Miller, L., Turner, T. J., Reeves, J. N., Lobban, A., Kraemer, S. B., Crenshaw, D. M., 2010, MNRAS, 403, 196
Muñoz-Darias, T., Motta, S., Pawar, D., Belloni, T. M., Campana, S., & Bhattacharya, D. 2010, MNRAS, 404, L94
Nowak, M. A., Vaughan, B. A., Wilms, J., Dove, J. B., Begelman, M. C., 1999, ApJ, 510, 874
O'Neill, P. M., Nandra, K., Papadakis, I. E., & Turner, T. J. 2005, MNRAS, 358, 1405
Orosz, J. A., McClintock, J. E., Aufdenberg, J. P., et al. 2011, ApJ, 742, 84
Paltani, S., Türler, M. 2005, A&A, 435, 811
Panessa, F., Bassani, L., Cappi, M., Dadina, M., Barcons, X., Carrera, F. J., Ho, L. C., & Iwasawa, K. 2006, A&A, 455, 173
Papadakis, I. E., Brinkmann, W., Negoro, H., & Gliozzi, M. 2002, A&A, 382, L1

Papadakis, I. E. 2004, MNRAS, 348, 207
Papadakis, I. E., Brinkmann, W., Gliozzi, M., & Raeth, C. 2010, A&A, 518, A28
Percival, D. B., and A. T. Walden 1993, *Spectral analysis for physical applications : multitaper and conventional univariate techniques*, Cambridge University Press, Cambridge.
Peterson, B. M., Bentz, M. C., Desroches, L. B., et al. 2005, ApJ, 632, 799
Peterson, B. M., Ferrarese, L., Gilbert, K. M., et al. 2004, ApJ, 613, 682
Piconcelli, E., Jimenez-Bailón, E., Guainazzi, M., et al. 2004, MNRAS, 351, 161
Ponti, G., Papadakis, I., Bianchi, S., et al. 2011, arXiv:1112.2744
Ponti, G., Miniutti, G., Cappi, M., Maraschi, L., Fabian, A. C., & Iwasawa, K. 2006, MNRAS, 368, 903
Pounds, K., Edelson, R., Markowitz, A., Vaughan, S., 2001, ApJ, 550, L15
Priestley, M. B. 1981, *Spectral Analysis and Time Series*, Academic Press, London.
Protassov, R., van Dyk, D. A., Connors, A., Kashyap, V. L., & Siemiginowska, A. 2002, ApJ, 571, 545
Ptak, A., Yaqoob, T., Mushotzky, R., Serlemitsos, P., & Griffiths, R. 1998, ApJ, 501, L37
Reid, M. J., McClintock, J. E., Narayan, R., et al. 2011, ApJ, 742, 83
Remillard, R. A., & McClintock, J. E. 2006, ARA&A, 44, 49
Revnivtsev, M., Gilfanov, M., & Churazov, E. 2000, A&A, 363, 1013
Shakura N. I., Sunyaev R. A., 1976, MNRAS, 175, 613
Shih, D. C., Iwasawa, K., & Fabian, A. C. 2003, MNRAS, 341, 973
Shu, X. W., Yaqoob, T., & Wang, J. X. 2010, ApJS, 187, 581
Sobolewska, M. A., & Papadakis, I. E. 2009, MNRAS, 399, 1597
Strüder, L., et al. 2001, A&A, 365, L18
Summons, D. P., Arévalo, P., McHardy, I. M., Uttley, P., & Bhaskar, A. 2007, MNRAS, 378, 649
Tomsick, J. A., Kalemci, E., Kaaret, P., 2004, ApJ, 601, 439
Tremaine, S., et al. 2002, ApJ, 574, 740
Urry, C. M., et al. 1993, ApJ, 411, 614
Uttley, P., McHardy, I. M., & Papadakis, I. E. 2002, MNRAS, 332, 231
Uttley, P., & McHardy, I. M. 2005, MNRAS, 363, 586
Uttley, P., Wilkinson, T., Cassatella, P., Wilms, J., Pottschmidt, K., Hanke, M., Bck, M., 2011, MNRAS, 414, L60
Vasudevan, R. V., & Fabian, A. C. 2009, MNRAS, 392, 1124
Vaughan, S., Edelson, R., Warwick, R. S., & Uttley, P. 2003A, MNRAS, 345, 1271
Vaughan, S., Fabian, A. C., & Nandra, K. 2003B, MNRAS, 339, 1237
Vaughan, S., & Fabian, A. C. 2003, MNRAS, 341, 496
Vaughan, S., Iwasawa, K., Fabian, A. C., & Hayashida, K. 2005, MNRAS, 356, 524
Vaughan S., Uttley P., 2005, MNRAS, 362, 235
Vaughan, S. 2010, MNRAS, 402, 307
Vaughan, S., Uttley, P., Pounds, K. A., Nandra, K., & Strohmayer, T. E. 2011, MNRAS, 413, 2489
Véron-Cetty, M.-P., & Véron, P. 2010, A&A, 518, A10
Watabe, Y., Kawakatu, N., Imanishi, M., & Takeuchi, T. T. 2009, MNRAS, 400, 1803
Watson, M. G., Schröder, A. C., Fyfe, D., et al. 2009, A&A, 493, 339
Wilms, J., Nowak, M. A., Pottschmidt, K., Pooley, G. G., & Fritz, S. 2006, A&A, 447, 245
Woo, J.-H., & Urry, C. M. 2002, ApJ, 579, 530
Zhang, X.-H., & Bao, G. 1991, A&A, 246, 21
Zhou, X.-L., & Wang, J.-M. 2005, ApJ, 618, L83
Zhou, X.-L., & Zhao, Y.-H. 2010, ApJ, 720, L206
Zoghbi, A., Fabian, A. C., Uttley, P., Miniutti, G., Gallo, L. C., Reynolds, C. S., Miller, J. M., & Ponti, G. 2010, MNRAS, 401, 2419

Num (1)	Name (2)	Type (3)	z (4)	$log(M_{BH})$ (5)	$log(L_{bol})$ (6)	Ref. (7)	ObsID (8)	Expos. (9)	L(2-10 keV) (10)	Var. (11)
1	Mrk335	NLSY1	0.0258	7.3	44.7	(1)	306870101	114.5	43.4	(TSH)
							600540501	80.5	42.9	(TSH)
							0601	130.1	42.9	(TSH)
2	IZw1	NLSY1	0.0611	7.4	45.1	(2)	300470101	79.8	43.6	(TSH)
3	NGC315	L2	0.0149	7.2	43.3	(3)	305290201	46.6	41.9	(NNN)
4	PGC643840	S1.0	0.1650	8.9	45.8	(2)	205680101	97.9	44.3	(NNN)
							401930101	41.8	44.3	(NNN)
5	ESO113-G10	S1.8	0.0260		44.2	(2)	301890101	94.8	42.7	(TSH)
6	Fairall9	S1.2	0.0470	8.4	45.2	(1)	605800401	129.3	43.9	(TSH)
7	NGC526A	S1.9	0.0191	7.9	44.3	(4)	150940101	41.3	43.3	(TSH)
8	RXJ0136.9-3510	NLSY1	0.2890	7.9	45.8	(2)	303340101	44.1	44.4	(TSH)
9	3C59	QSO	0.2410				205390201	67.4	44.4	(NNN)
10	Mrk586	NLSY1	0.1553	7.6	45.5	(2)	048740101	41.2	44.3	(TSH)
11	Mrk590	S1.0	0.0264	7.7	44.6	(2)	201020201	44.8	43.1	(NNN)
12	Mrk1040	S1.0	0.016	7.6	44.5	(2)	554990101	88.4	43.0	(TSH)
13	NGC985	S1.5	0.0431	8.1	45.1	(2)	150470601	54.4	43.7	(NNH)
14	NGC1052	L2	0.0049	8.2		(5)	306230101	49.9	41.4	(NNN)
							553300301	50.2	41.5	(NNN)
							0401	56.9	41.5	(NNN)
15	NGC1365	S1.8	0.0045	7.6	43.8	(4)	205590301	54.5	41.9	(TNH)
							0401	63.4	41.6	(TNH)
							505140401	121.7	40.9	(TNH)
16	PGC013424	L2	0.0350				147800201	89.9	43.5	(NNN)
17	2E0414+0057	BL	0.2870				161160101	75.7	45.1	(NNH)
18	3C111	S1.0	0.049				552180101	116.0	44.5	(TSH)
19	1H0419-577	S1.5	0.104	6.3	44.1	(2)	604720301	106.0	44.6	(TSN)
							0401	60.2	44.5	(TSN)
20	3C120	S1.5	0.0330	7.7	45.5	(2)	152840101	114.8	44.1	(TSH)
21	2E0507+1626	S1.5	0.0170				502090501	55.3	43.2	(TSH)
22	Ark120	S1.0	0.0327	8.2	44.9	(2)	147190101	98.4	44.0	(TSH)
23	MCG-02-14-009	S1.0	0.02845		44.4	(2)	550640101	117.4	43.0	(TSH)
24	ESO362-G18	S1.5	0.01245				610180101	76.2	42.5	(TSH)
25	PKS0518-45	L1	0.0351				206390101	48.6	43.5	(NNN)
26	PKS0548-322:G4	S1.0	0.0720				142270101	85.2	43.7	(TSN)
27	PKS0548-322	BL	0.0748	8.1		(6)	142270101	79.8	44.4	(TSH)
28	NGC2110	S1.0	0.0078	8.3	43.5	(4)	145670101	42.7	42.6	(NNN)
29	PKS0558-504	NLSY1	0.13720	8.5	46.8	(1)	555170201	120.8	44.8	(TSH)
							0301	125.8	44.8	(TSH)
							0401	123.1	44.9	(TSH)
							0501	124.2	44.8	(TSH)
							0601	115.1	44.9	(TSH)
30	Mrk3	S2.0	0.0135	8.6	44.8	(4)	111220201	53.0	42.4	(NNN)
31	1H0707-495	NLSY1	0.0410	6.4	44.4	(1)	148010301	74.7	42.8	(TSH)
							511580101	118.5	42.8	(TSH)
							0201	99.0	42.8	(TSH)
							0301	100.9	42.7	(TSH)
							0401	98.7	42.7	(TSH)
							653510301	109.8	42.6	(TSH)
							0401	121.8	42.6	(TSH)
							0501	116.8	42.7	(TSH)
							0601	119.4	42.5	(TSH)
							554710801	95.8	42.6	(TSH)
32	Mrk79	S1.2	0.02219				502091001	74.8	43.1	(TSN)
33	PG0804+761	S1.0	0.10000				605110101	42.8	44.7	(TSH)
34	OJ+287	BL	0.3060				401060201	41.9	44.7	(NNN)
							502630201	46.8	44.7	(TSN)
35	Mrk704	S1.2	0.02923	8.1	44.8	(2)	502091601	97.5	43.3	(TSH)
36	NGC2992	S1.9	0.00712				654910301	58.7	41.9	(NNN)
							0401	57.3	41.9	(TNH)
							0501	55.2	42.2	(TSH)
							0601	55.2	41.8	(TNH)
							0701	55.2	41.8	(NNN)
							0801	50.9	41.7	(NNN)
							0901	55.3	41.6	(TNN)
							1001	59.8	41.8	(TSH)
37	3C218	L2	0.0549	9.2		(7)	504260101	115.0	43.8	(TNN)
38	Mrk110	NLSY1	0.0353	7.4	44.7	(2)	201130501	43.8	43.9	(TSH)
39	ESO434-G40	S1.0	0.0085	6.3	44.3	(1)	302850201	104.8	43.2	(TSH)
40	NGC3031	L1	0.0009	7.9		(6)	111800101	74.8	40.3	(TSN)
41	S40954+6533	BL	0.3670				502430201	52.4	45.1	(TSH)
42	NGC3227	S1.5	0.0052	6.9	43.9	(1)	400270101	94.7	42.3	(TSH)
43	1ES1028+511	BL	0.3610				303720201	88.2	45.6	(TSH)
							0301	97.8	45.7	(TSH)
							0601	89.8	45.5	(TSH)
44	HE1029-1401	S1.0	0.0860	8.7	46.0	(2)	203770101	42.5	44.6	(TSH)
45	KUG1031+398	NLSY1	0.0420	6.6	44.8	(1)	506440101	88.1	42.6	(TSH)
							561580201	49.8	43.0	(TSN)
							655310101	41.8	43.3	(TSH)
							0201	52.8	43.3	(TSH)
46	RXJ1054.3+5725	S1.0	0.2050				147511301	69.8	44.4	(NNN)
47	NGC3516	S1.5	0.0097	7.5	44.3	(1)	107460601	89.8	42.8	(TSH)
							0701	119.8	43.0	(TSH)
							401210401	48.6	42.5	(TSH)
							0501	65.6	42.9	(TSH)
							0601	64.9	43.0	(TSH)

Num (1)	Name (2)	Type (3)	z (4)	$log(M_{BH})$ (5)	$log(L_{bol})$ (6)	Ref. (7)	ObsID (8)	Expos. (9)	L(2-10 keV) (10)	Var. (11)
							1001	54.8	43.0	(TSH)
48	PG1116+215	S1.0	0.1770	8.5	46.0	(2)	201940101	84.8	44.5	(NNN)
							554380101	74.8	44.5	(TSN)
							0201	66.8	44.5	(TSH)
							0301	69.8	44.5	(TSH)
49	NGC3783	S1.5	0.0096	7.5	44.4	(1)	112210201	68.8	43.0	(TSH)
							0501	119.8	42.9	(TSH)
50	NGC4051	NLSY1	0.0036	6.1	43.6	(1)	109141401	99.8	41.8	(TSH)
							157560101	46.8	41.2	(TSH)
							606320101	45.0	41.2	(TSH)
							0201	44.1	41.2	(TSH)
							1601	41.2	41.2	(TSH)
							1901	39.1	41.2	(TSH)
							2201	40.9	41.2	(TSH)
							2301	42.0	41.2	(TSH)
51	NGC4151	S1.5	0.0030	7.1	43.7	(1)	112830201	53.9	42.4	(TNH)
							402660201	45.1	42.0	(TNH)
52	PG1211+143	NLSY1	0.0820	7.6	45.8	(2)	112610101	49.9	43.9	(TSH)
							208020101	47.7	43.9	(TSH)
							502050101	55.4	43.7	(TSH)
53	Mrk766	NLSY1	0.0129	6.6	44.1	(1)	109141301	125.0	42.5	(TSH)
							304030101	91.7	42.6	(TSH)
							0301	95.3	42.8	(TSH)
							0401	98.2	42.7	(TSH)
							0501	91.9	43.0	(TSH)
							0601	98.2	42.8	(TSH)
54	NGC4258	S2.0	0.0019	7.6	43.5	(5)	400560301	59.6	40.6	(NNH)
55	NGC4261	L2	0.0080	8.7	41.8	(8)	502120101	115.8	41.3	(NNN)
56	Mrk205	S1.0	0.0708	8.3	45.6	(2)	401240301	52.2	44.1	(TSH)
							0501	49.8	44.2	(NNN)
57	NGC4395	S1.8	0.0010	5.6	41.4	(1)	142830101	103.1	40.2	(TSH)
58	3C273	S1.0	0.1583	8.9	47.3	(2)	126700301	54.8	45.9	(NNN)
							0801	57.6	45.8	(TSH)
							136550101	85.3	45.7	(TSN)
							159960101	54.8	45.7	(NNN)
							414190101	73.6	45.8	(TSH)
							0801	43.2	45.7	(TSH)
59	NGC4472	L1	0.0040	8.8		(7)	200130101	77.8	40.3	(NNN)
60	NGC4486	L2	0.0042	9.6	42.0	(8)	200920101	69.8	41.9	(NNN)
61	LBQS1228+1116	QSO	0.2370		45.8	(2)	306630101	67.8	44.4	(NNN)
							0201	92.8	44.3	(NNN)
62	MS1229.2+6430	BL	0.1640				124900101	44.8	44.3	(NNN)
63	NGC4593	S1.0	0.0110	6.7	44.3	(2)	059830101	73.0	43.0	(TSH)
64	NGC4636	L2.0	0.0040	8.2		(7)	111190701	56.0	39.7	(NNN)
65	NGC4696	L2	0.0094	8.6		(7)	046340101	41.5	41.8	(NNN)
66	NGC4736	L1.8	0.0012	7.0		(7)	404980101	49.5	40.0	(NNN)
67	XCom	S1.5	0.0910				204040101	84.5	43.6	(NNN)
							0201	92.2	43.7	(TSH)
							0301	91.8	43.7	(TSN)
							304320201	54.8	43.6	(NNN)
							0301	50.2	43.6	(TSH)
							0801	58.8	43.8	(TSH)
68	MCG-03-34-064	S2.0	0.0165	7.8	44.7	(4)	506340101	85.7	42.4	(TNH)
69	IRAS13224-3809	S1.0	0.0658	6.8	42.8	(2)	110890101	57.8	42.8	(TSH)
70	MCG-06-30-015	NLSY1	0.0077	6.7	43.8	(1)	029740101	80.3	42.8	(TSH)
							0701	123.6	42.7	(TSH)
							0801	121.5	42.8	(TSH)
							111570201	51.9	42.8	(TSH)
71	IRAS13349+2438	NLSY1	0.1070	7.7	45.5	(2)	096010101	40.9	43.9	(TSH)
							402080301	59.8	44.2	(TSH)
72	NGC5252	S2.0	0.0230	8.0		(5)	152940101	59.0	43.2	(NNN)
73	PKS1346+26	L2	0.0630	8.6	46.1	(2)	097820101	44.7	44.0	(NNN)
74	IC4329A	S1.2	0.0160	8.3	45.5	(1)	147440101	125.0	43.8	(TSH)
75	Mrk279	S1.0	0.0305	7.5	45.3	(2)	302480401	56.2	43.8	(TSN)
							0501	56.1	43.8	(NNN)
76	PG1351+640	S1.5	0.0870	7.7	45.5	(2)	205390301	45.6	43.1	(NNN)
77	Circinus	S2.0	0.0011	6.2	43.6	(9)	111240101	98.0	40.5	(TSH)
78	NGC5506	S1.9	0.00674	7.4	44.0	(1)	554170101	88.2	43.1	(TSH)
							0201	90.2	43.1	(TSH)
79	NGC5548	S2.0	0.0172	7.6	44.8	(1)	089960301	79.8	43.5	(TSH)
80	PG1416-129	S1.2	0.1293	9.1	45.6	(2)	203770201	45.1	44.2	(NNN)
81	ESO511-G030	S1.0	0.0224	8.7	44.8	(2)	502090201	105.7	43.4	(TSH)
82	TON0202	S1.2	0.3660				111290601	47.8	45.0	(NNN)
83	RBS1399	BL	0.1290				111850201	63.1	45.0	(TSH)
							165770101	62.4	45.1	(NNN)
							0201	65.4	45.1	(TSN)
							310190101	43.6	45.0	(TSH)
							0201	42.0	45.3	(TSN)
84	Mrk841	S1.5	0.0364	8.5	45.8	(2)	205340201	42.9	43.5	(TSH)
85	PKS1549-79	S2.0	0.15220				550970101	84.6	44.7	(TNH)
86	NGC6251	L2.0	0.0247	9.0		(7)	056340201	42.7	42.8	(NNN)
87	PDS456	QSO	0.1840	8.9	46.3	(2)	501580101	85.7	44.6	(TSH)
							0201	82.4	44.8	(TSH)
88	3C390.3	S1.5	0.0561	8.5	45.9	(2)	203720201	48.4	44.5	(NNN)
89	ESO141-G55	S1.2	0.0371				503750101	74.6	43.9	(TSH)

Num (1)	Name (2)	Type (3)	z (4)	$log(M_{BH})$ (5)	$log(L_{bol})$ (6)	Ref. (7)	ObsID (8)	Expos. (9)	L(2-10 keV) (10)	Var. (11)
90	NGC6860	S1.5	0.01488	7.6	44.5	(2)	552170301	114.8	43.1	(TSH)
91	Mrk509	S1.5	0.0344	8.1	45.0	(2)	306090201	82.3	44.1	(TSH)
							0301	43.2	44.0	(TSH)
							0401	66.3	44.0	(TSH)
							601390201	55.8	44.1	(TSH)
							0301	63.1	44.1	(TSH)
							0401	60.2	44.1	(TSH)
							0501	60.2	44.1	(TSH)
							0601	62.1	44.1	(TSH)
							0701	62.4	44.1	(TSH)
							0801	60.2	44.2	(TSH)
							0901	60.2	44.1	(TSH)
							1001	64.8	44.1	(TSH)
							1101	62.1	44.1	(TSH)
92	IGRJ21277+5656	NLSY1	0.01440				655450101	130.3	43.0	(TSH)
93	CTSA08.12	S1.2	0.0300		44.7	(2)	201130301	42.8	43.2	(NNN)
94	PKS2135-14	S1.5	0.2000	8.9	46.2	(4)	092850201	52.4	44.8	(TSH)
							080940101	54.2	44.9	(TSH)
							0301	55.1	45.3	(TSH)
							124930201	56.2	44.8	(TSH)
							0301	41.5	45.0	(TSH)
							0601	53.7	44.8	(TSH)
							158961301	56.7	45.1	(TSH)
							1401	61.3	45.2	(TSH)
							411780201	64.4	45.2	(TSH)
							0401	64.1	45.0	(TSH)
							0501	66.8	44.7	(TSH)
							0601	63.1	45.0	(TSH)
95	NGC7172	S2.0	0.0085	8.2	43.8	(4)	202860101	53.4	42.7	(TNH)
96	NGC7213	S1.5	0.00514	7.7	44.3	(2)	605800301	125.4	41.9	(TSN)
97	NGC7314	S2.0	0.0048	6.7	43.8	(2)	311190101	78.9	41.9	(TSH)
98	Ark564	NLSY1	0.0247	6.9	44.9	(1)	206400101	95.8	43.4	(TSH)
99	3C452	S2.0	0.08110				552580201	66.5	43.6	(NNN)
100	2REJ2248-511	S1.5	0.1020	8.1	45.5	(2)	510380101	61.3	44.1	(NNN)
101	MR2251-178	S1.5	0.0640	8.0	45.8	(2)	012940101	60.8	44.3	(NNN)
102	MS22549-3712	S1.9	0.0390	6.6	44.3	(2)	205390101	67.8	43.1	(TSH)
103	NGC7469	S1.5	0.0163	7.4	44.6	(1)	207090101	81.4	43.3	(TSH)
							0201	75.4	43.2	(TSH)
104	NGC7582	S2.0	0.0052	7.7	43.3	(4)	204610101	84.8	41.2	(TSH)

Table 1. Sample main observational properties. References for BH masses and bolometric luminosities: (1) See references in Tab. 4, (2) Ponti et al. (2011) and references therein, (3) Gu et al. (2007), (4) Vasudevan & Fabian (2009), (5) Woo & Urry (2002), (6) Gültekin et al. (2009), (7) BH mass obtained using the relation derived by Tremaine et al. (2002), (8) Eracleous et al. (2010), and (9) Greenhill et al. (2003).

Name	ObsID	0.2-10 keV		0.2-2 keV		2-10 keV	
		log(N)	α	log(N)	α	log(N)	α
(1)	(2)	(3)	(4)	(5)	(6)	(7)	(8)
Mrk335	306870101	$-9.1^{+0.5}_{-0.5}$	$2.7^{+0.2}_{-0.1}$	$-8.9^{+0.5}_{-0.5}$	$2.6^{+0.2}_{-0.1}$	$-6.2^{+0.6}_{-0.6}$	$2.0^{+0.2}_{-0.2}$
	600540501	$-7.8^{+0.4}_{-0.4}$	$2.4^{+0.1}_{-0.1}$	$-7.6^{+0.4}_{-0.4}$	$2.3^{+0.1}_{-0.1}$	$-6.2^{+0.6}_{-0.8}$	$2.0^{+0.2}_{-0.2}$
	0601						
IZw1	300470101	$-8.2^{+0.8}_{-0.9}$	$2.4^{+0.2}_{-0.2}$	$-8.2^{+0.8}_{-0.9}$	$2.4^{+0.2}_{-0.2}$	$-5.4^{+1.1}_{-1.3}$	$1.7^{+0.3}_{-0.3}$
ESO113-G10	301890101	$-6.6^{+0.5}_{-0.6}$	$2.0^{+0.2}_{-0.2}$	$-6.4^{+0.5}_{-0.6}$	$2.0^{+0.2}_{-0.2}$	$-5.1^{+0.8}_{-0.9}$	$1.7^{+0.2}_{-0.2}$
Fairall9	605800401	$-7.8^{+0.8}_{-0.8}$	$2.1^{+0.2}_{-0.2}$	$-7.8^{+0.8}_{-0.8}$	$2.1^{+0.2}_{-0.2}$	$-7.8^{+1.2}_{-1.5}$	$2.0^{+0.3}_{-0.3}$
NGC526A	150940101	$-13.4^{+4.0}_{\clubsuit}$	$3.3^{+1.3}_{-1.0}$	$-13.9^{\clubsuit}$	$3.5^{+1.7}_{-1.2}$	$-11.8^{+3.5}_{\clubsuit}$	$3.0^{+1.2}_{-0.8}$
RXJ0136.9-3510	303340101	$-6.7^{+0.8}_{-0.9}$	$2.0^{+0.3}_{-0.2}$	$-6.7^{+0.8}_{-0.9}$	$2.0^{+0.3}_{-0.2}$	$-4.8^{+1.5}_{-1.9}$	$1.7^{+0.5}_{-0.4}$
Mrk586	048740101	$-10.1^{+1.3}_{-1.5}$	$2.9^{+0.4}_{-0.3}$	$-9.7^{+1.3}_{-1.5}$	$2.8^{+0.4}_{-0.3}$	$-6.3^{+2.2}_{-2.5}$	$2.0^{+0.6}_{-0.5}$
Mrk1040	554990101	$-8.5^{+0.8}_{-0.8}$	$2.4^{+0.2}_{-0.2}$	$-8.7^{+0.8}_{-0.9}$	$2.4^{+0.2}_{-0.2}$	$-8.0^{+0.9}_{-1.0}$	$2.2^{+0.3}_{-0.2}$
NGC985	150470601					$-6.3^{+3.5}_{\clubsuit}$	$1.7^{\clubsuit}_{-0.8}$
NGC1365	205590301	$-3.1^{+0.4}_{-0.4}$	$1.2^{+0.1}_{-0.1}$			$-3.1^{+0.2}_{-0.2}$	$1.3^{+0.1}_{-0.1}$
	0401						
	505140401	$-2.2^{+0.6}_{-0.8}$	$0.8^{+0.2}_{-0.2}$			$-8.0^{+2.4}_{-3.3}$	$2.2^{+0.8}_{-0.5}$
2E0414+0057	161160101					$-6.6^{+2.5}_{-3.6}$	$1.9^{+0.8}_{-0.6}$
3C111	552180101	$-7.6^{+1.5}_{-1.9}$	$1.8^{+0.4}_{-0.3}$	$-6.6^{+2.0}_{-4.0}$	$1.5^{+0.8}_{-0.5}$	$-8.4^{+1.7}_{-2.0}$	$2.0^{+0.5}_{-0.4}$
1H0419-577	604720301	$-14.2^{+2.3}_{-3.0}$	$3.2^{+0.6}_{-0.5}$	$-14.1^{+2.3}_{-2.9}$	$3.2^{+0.6}_{-0.5}$		
	0401						
3C120	152840101	$-8.4^{+0.8}_{-0.9}$	$2.2^{+0.2}_{-0.2}$	$-8.5^{+0.8}_{-1.0}$	$2.2^{+0.2}_{-0.2}$	$-7.4^{+1.1}_{-1.5}$	$1.9^{+0.3}_{-0.3}$
2E0507+1626	502090501	$-7.0^{+1.0}_{-1.2}$	$1.9^{+0.3}_{-0.3}$	$-7.4^{+1.2}_{-1.5}$	$2.0^{+0.4}_{-0.3}$	$-7.5^{+1.5}_{-2.2}$	$2.0^{+0.5}_{-0.4}$
Ark120	147190101	$-17.0^{\clubsuit}$	$3.7^{+2.3}_{-1.5}$	$-18.1^{\clubsuit}$	$3.9^{+2.2}_{-1.3}$	$-9.3^{+2.9}_{\clubsuit}$	$2.1^{+1.1}_{-0.6}$
MCG-02-14-009	550640101	$-5.8^{+0.5}_{-0.5}$	$1.8^{+0.1}_{-0.1}$	$-5.3^{+0.4}_{-0.5}$	$1.7^{+0.1}_{-0.1}$	$-6.9^{+1.1}_{-1.3}$	$2.0^{+0.3}_{-0.3}$
ESO362-G18	610180101	$-9.4^{+1.0}_{-1.2}$	$2.6^{+0.3}_{-0.3}$	$-9.6^{+1.1}_{-1.3}$	$2.7^{+0.3}_{-0.3}$	$-8.6^{+1.6}_{-2.2}$	$2.4^{+0.5}_{-0.4}$
PKS0548-322:G4	142270101	$-5.7^{+0.8}_{-0.9}$	$1.9^{+0.2}_{-0.2}$	$-5.5^{+0.8}_{-0.9}$	$1.9^{+0.2}_{-0.2}$		
PKS0548-322	142270101	$-22.2^{\clubsuit}$	$4.7^{+2.9}_{-1.7}$	$-51.2^{\clubsuit}$	$10.5^{\clubsuit}_{-3.1}$	$-13.0^{\clubsuit}$	$2.9^{+2.0}_{-1.3}$
PKS0558-504	555170201	$-7.9^{+0.2}_{-0.2}$	$2.3^{+0.1}_{-0.1}$	$-7.9^{+0.2}_{-0.2}$	$2.3^{+0.1}_{-0.1}$	$-7.2^{+0.3}_{-0.3}$	$2.2^{+0.1}_{-0.1}$
	0301						
	0401						

Name	ObsID	0.2-10 keV		0.2-2 keV		2-10 keV	
		log(N)	α	log(N)	α	log(N)	α
(1)	(2)	(3)	(4)	(5)	(6)	(7)	(8)
	0501						
	0601						
1H0707-495	148010301	-4.4 $^{+0.3}_{-0.4}$	1.7 $^{+0.1}_{-0.1}$	-4.5 $^{+0.3}_{-0.4}$	1.7 $^{+0.1}_{-0.1}$	-2.2 $^{+0.6}_{-0.6}$	1.2 $^{+0.2}_{-0.2}$
	511580101	-5.4 $^{+0.2}_{-0.2}$	2.0 $^{+0.1}_{-0.1}$	-5.5 $^{+0.2}_{-0.2}$	2.0 $^{+0.1}_{-0.1}$	-3.0 $^{+0.2}_{-0.3}$	1.4 $^{+0.1}_{-0.1}$
	0201						
	0301						
	0401						
	653510301	-5.9 $^{+0.1}_{-0.1}$	2.2 $^{+0.0}_{-0.0}$	-6.1 $^{+0.1}_{-0.1}$	2.2 $^{+0.1}_{-0.0}$	-3.0 $^{+0.2}_{-0.2}$	1.5 $^{+0.1}_{-0.1}$
	0401						
	0501						
	0601						
	554710801	-4.4 $^{+0.4}_{-0.5}$	1.8 $^{+0.1}_{-0.1}$	-4.5 $^{+0.4}_{-0.5}$	1.8 $^{+0.1}_{-0.1}$	-2.2 $^{+0.8}_{-0.9}$	1.3 $^{+0.2}_{-0.2}$
Mrk79	502091001	-7.5 $^{+1.8}_{-2.5}$	1.9 $^{+0.6}_{-0.4}$	-6.4 $^{+1.3}_{-1.6}$	1.7 $^{+0.4}_{-0.3}$		
PG0804+761	605110101	-5.0 $^{+1.3}_{-1.6}$	1.2 $^{+0.4}_{-0.3}$	-5.2 $^{+2.2}_{-3.5}$	1.2 $^{+0.9}_{-0.5}$	-4.7 $^{+1.2}_{-1.4}$	1.6 $^{+0.4}_{-0.3}$
OJ+287	502630201	-5.7 $^{+2.0}_{-2.6}$	1.6 $^{+0.6}_{-0.5}$	-6.0 $^{+2.2}_{-3.2}$	1.6 $^{+0.8}_{-0.6}$		
Mrk704	502091601	-8.8 $^{+1.0}_{-1.1}$	2.3 $^{+0.3}_{-0.2}$	-8.5 $^{+0.9}_{-1.1}$	2.2 $^{+0.3}_{-0.2}$	-9.4 $^{+2.2}_{-2.8}$	2.4 $^{+0.6}_{-0.5}$
NGC2992	654910401	-6.9 $^{+0.9}_{-1.1}$	1.9 $^{+0.3}_{-0.2}$			-7.2 $^{+1.2}_{-1.4}$	2.0 $^{+0.3}_{-0.3}$
	0501						
	0601						
	0901						
	1001						
3C218	504260101	-10.5 $^{\clubsuit}$	2.2 $^{+1.9}_{-1.5}$				
Mrk110	201130501	-13.3 $^{+2.6}_{-3.5}$	3.2 $^{+0.8}_{-0.6}$	-12.3 $^{+2.3}_{-2.9}$	2.9 $^{+0.8}_{-0.5}$	-21.7 $^{\clubsuit}$	5.1 $^{+3.5}_{-1.8}$
ESO434-G40	302850201	-9.1 $^{+0.8}_{-0.9}$	2.5 $^{+0.2}_{-0.2}$	-8.4 $^{+1.0}_{-1.1}$	2.3 $^{+0.3}_{-0.2}$	-9.1 $^{+0.8}_{-0.9}$	2.5 $^{+0.2}_{-0.2}$
NGC3031	111800101	-8.7 $^{+1.8}_{-2.2}$	2.1 $^{+0.5}_{-0.4}$	-8.2 $^{+1.9}_{-2.2}$	2.0 $^{+0.5}_{-0.4}$		
S40954+6533	502430201	-5.5 $^{+0.8}_{-0.9}$	1.8 $^{+0.2}_{-0.2}$	-5.4 $^{+0.8}_{-0.9}$	1.8 $^{+0.2}_{-0.2}$	0.3 $^{+0.9}_{-2.3}$	0.3 $^{+0.6}_{-0.2}$
NGC3227	400270101	-7.7 $^{+0.4}_{-0.5}$	2.3 $^{+0.1}_{-0.1}$	-7.6 $^{+0.5}_{-0.5}$	2.3 $^{+0.1}_{-0.1}$	-6.5 $^{+0.6}_{-0.6}$	2.0 $^{+0.2}_{-0.2}$
1ES1028+511	303720201	-8.9 $^{+1.3}_{-1.6}$	2.0 $^{+0.3}_{-0.3}$	-9.3 $^{+1.6}_{-2.2}$	2.1 $^{+0.5}_{-0.3}$	-9.4 $^{+1.8}_{-2.2}$	2.5 $^{+0.5}_{-0.4}$
	0301						
	0601						
HE1029-1401	203770101	-4.6 $^{+1.2}_{-1.4}$	1.1 $^{+0.4}_{-0.3}$	-4.3 $^{+1.3}_{-1.5}$	1.0 $^{+0.4}_{-0.3}$	-1.8 $^{+1.8}_{-3.2}$	0.5 $^{+0.8}_{-0.4}$
KUG1031+398	506440101	-5.3 $^{+0.5}_{-0.6}$	1.6 $^{+0.2}_{-0.2}$	-5.3 $^{+0.5}_{-0.6}$	1.6 $^{+0.2}_{-0.2}$	-0.6 $^{+1.2}_{-1.1}$	0.5 $^{+0.3}_{-0.3}$
	561580201	-3.4 $^{+0.7}_{-0.8}$	1.0 $^{+0.2}_{-0.2}$	-3.6 $^{+0.8}_{-0.9}$	1.0 $^{+0.2}_{-0.2}$		
	655310101	-4.9 $^{+0.5}_{-0.6}$	1.5 $^{+0.2}_{-0.2}$	-5.0 $^{+0.5}_{-0.6}$	1.5 $^{+0.2}_{-0.2}$	-3.0 $^{+0.8}_{-0.9}$	1.5 $^{+0.2}_{-0.2}$
	0201						
NGC3516	107460601	-10.1 $^{+1.1}_{-1.3}$	2.5 $^{+0.3}_{-0.2}$	-10.2 $^{+1.3}_{-1.6}$	2.6 $^{+0.3}_{-0.3}$	-10.2 $^{+1.4}_{-1.7}$	2.6 $^{+0.4}_{-0.3}$
	0701						
	401210401	-9.1 $^{+0.4}_{-0.4}$	2.6 $^{+0.1}_{-0.1}$	-9.1 $^{+0.4}_{-0.4}$	2.7 $^{+0.1}_{-0.1}$	-8.3 $^{+0.5}_{-0.6}$	2.4 $^{+0.1}_{-0.1}$
	0501						
	0601						
	1001						
PG1116+215	554380101	-9.5 $^{+1.1}_{-1.3}$	2.3 $^{+0.3}_{-0.3}$	-9.6 $^{+1.2}_{-1.5}$	2.4 $^{+0.3}_{-0.3}$		
	0201						
	0301						
NGC3783	112210201	-7.9 $^{+0.4}_{-0.5}$	2.2 $^{+0.1}_{-0.1}$	-8.1 $^{+0.5}_{-0.5}$	2.3 $^{+0.1}_{-0.1}$	-7.5 $^{+0.6}_{-0.6}$	2.1 $^{+0.2}_{-0.1}$
	0501						
NGC4051	109141401	-5.1 $^{+0.3}_{-0.3}$	2.0 $^{+0.1}_{-0.1}$	-4.6 $^{+0.2}_{-0.2}$	1.9 $^{+0.1}_{-0.1}$	-3.5 $^{+0.2}_{-0.2}$	1.5 $^{+0.1}_{-0.1}$
	157560101	-6.3 $^{+0.4}_{-0.4}$	2.3 $^{+0.1}_{-0.1}$	-6.3 $^{+0.4}_{-0.4}$	2.3 $^{+0.1}_{-0.1}$	-5.4 $^{+0.6}_{-0.6}$	2.1 $^{+0.2}_{-0.2}$
	606320101	-5.4 $^{+0.2}_{-0.2}$	2.1 $^{+0.1}_{-0.1}$	-5.3 $^{+0.2}_{-0.2}$	2.0 $^{+0.1}_{-0.1}$	-4.5 $^{+0.2}_{-0.3}$	1.8 $^{+0.1}_{-0.1}$
	0201						
	1601						
	1901						
	2201						
	2301						
NGC4151	112830201	-21.8 $^{\clubsuit}$	5.0 $^{+2.0}_{-1.7}$			-10.6 $^{+2.0}_{-3.2}$	2.7 $^{+0.8}_{-0.4}$
	402660201	-7.8 $^{+1.1}_{-1.3}$	2.1 $^{+0.3}_{-0.3}$			-8.3 $^{+1.2}_{-1.5}$	2.3 $^{+0.4}_{-0.3}$
PG1211+143	112610101	-9.8 $^{+1.5}_{-1.8}$	2.7 $^{+0.4}_{-0.4}$	-9.9 $^{+1.6}_{-2.0}$	2.7 $^{+0.5}_{-0.4}$	-8.5 $^{+2.0}_{-2.6}$	2.4 $^{+0.6}_{-0.5}$
	208020101	-5.9 $^{+0.6}_{-0.6}$	1.9 $^{+0.2}_{-0.2}$	-6.3 $^{+0.6}_{-0.8}$	2.1 $^{+0.2}_{-0.2}$	-5.0 $^{+0.9}_{-1.1}$	1.8 $^{+0.3}_{-0.2}$
	502050101	-8.6 $^{+0.8}_{-0.9}$	2.5 $^{+0.3}_{-0.2}$	-8.6 $^{+0.9}_{-1.0}$	2.5 $^{+0.3}_{-0.2}$	-7.6 $^{+1.5}_{-2.0}$	2.3 $^{+0.5}_{-0.4}$
Mrk766	109141301	-6.5 $^{+0.3}_{-0.3}$	2.1 $^{+0.1}_{-0.1}$	-6.6 $^{+0.3}_{-0.3}$	2.2 $^{+0.1}_{-0.1}$	-4.3 $^{+0.3}_{-0.3}$	1.6 $^{+0.1}_{-0.1}$
	304030101	-6.5 $^{+0.2}_{-0.2}$	2.1 $^{+0.1}_{-0.1}$	-6.5 $^{+0.2}_{-0.2}$	2.2 $^{+0.1}_{-0.1}$	-4.5 $^{+0.2}_{-0.2}$	1.6 $^{+0.1}_{-0.1}$
	0301						
	0401						
	0501						
	0601						
NGC4258	400560301*					-2.3 $^{\clubsuit}$	-0.7 $^{\clubsuit}$
Mrk205	401240301	-8.8 $^{+1.0}_{-1.1}$	2.2 $^{+0.3}_{-0.2}$	-8.8 $^{+1.1}_{-1.3}$	2.2 $^{+0.3}_{-0.3}$	-5.5 $^{+1.4}_{-2.0}$	1.5 $^{+0.4}_{-0.3}$
NGC4395	142830101*	-2.3 $^{+0.2}_{-0.2}$	1.3 $^{+0.1}_{-0.1}$	-8.8 $^{+0.8}_{-0.9}$	1.8 $^{+0.2}_{-0.2}$	-2.3 $^{+0.9}_{-2.3}$	0.3 $^{+0.6}_{-0.2}$
3C273	126700801	-7.9 $^{+1.6}_{-2.3}$	1.7 $^{+0.5}_{-0.4}$	-6.4 $^{+1.1}_{-1.5}$	1.4 $^{+0.4}_{-0.3}$	-15.9 $^{\clubsuit}$	3.5 $^{\clubsuit}_{-1.9}$
	136550101	-11.8 $^{+3.0}_{-3.6}$	2.5 $^{+0.8}_{-0.7}$	-12.2 $^{+3.2}_{-3.8}$	2.6 $^{+0.8}_{-0.7}$		
	414190101	-4.6 $^{+2.4}_{-2.8}$	0.9 $^{+0.6}_{-0.6}$	-4.6 $^{+2.4}_{-2.8}$	0.9 $^{+0.6}_{-0.6}$	-4.6 $^{+2.4}_{-2.8}$	0.9 $^{+0.6}_{-0.6}$
	0801						
NGC4593	059830101	-7.8 $^{+0.4}_{-0.5}$	2.3 $^{+0.1}_{-0.1}$	-7.9 $^{+0.5}_{-0.5}$	2.3 $^{+0.2}_{-0.1}$	-8.3 $^{+0.9}_{-1.0}$	2.4 $^{+0.3}_{-0.2}$
XCom	204040201	-5.8 $^{+0.4}_{-0.4}$	1.8 $^{+0.1}_{-0.1}$	-5.7 $^{+0.4}_{-0.4}$	1.8 $^{+0.1}_{-0.1}$	-4.8 $^{+1.1}_{-1.6}$	1.4 $^{+0.3}_{-0.3}$
	0301						
	304320301	-6.6 $^{+0.8}_{-1.0}$	1.8 $^{+0.2}_{-0.2}$	-6.9 $^{+0.9}_{-1.0}$	1.9 $^{+0.2}_{-0.2}$	-11.5 $^{\clubsuit}$	2.8 $^{+2.2}_{-1.2}$
	0801						
MCG-03-34-064	506340101	-8.5 $^{+2.9}_{\clubsuit}$	2.2 $^{+1.1}_{-0.6}$			-8.8 $^{+2.2}_{-3.0}$	2.5 $^{+0.8}_{-0.5}$
IRAS13224-3809	110890101	-5.1 $^{+0.3}_{-0.4}$	1.9 $^{+0.1}_{-0.1}$	-5.2 $^{+0.4}_{-0.4}$	1.9 $^{+0.1}_{-0.1}$	-3.0 $^{+0.8}_{-0.8}$	1.4 $^{+0.2}_{-0.2}$
MCG-06-30-015	029740101	-6.9 $^{+0.2}_{-0.2}$	2.3 $^{+0.1}_{-0.1}$	-6.9 $^{+0.2}_{-0.2}$	2.3 $^{+0.1}_{-0.1}$	-5.3 $^{+0.2}_{-0.2}$	1.8 $^{+0.1}_{-0.1}$
	0701						

Name	ObsID	0.2-10 keV		0.2-2 keV		2-10 keV	
		log(N)	α	log(N)	α	log(N)	α
(1)	(2)	(3)	(4)	(5)	(6)	(7)	(8)
	0801						
	111570201	$-7.3^{+0.5}_{-0.5}$	$2.4^{+0.2}_{-0.2}$	$-7.4^{+0.5}_{-0.5}$	$2.4^{+0.2}_{-0.2}$	$-5.2^{+0.5}_{-0.5}$	$1.8^{+0.2}_{-0.2}$
IRAS13349+2438	096010101	$-6.9^{+0.8}_{-0.9}$	$2.1^{+0.2}_{-0.2}$	$-7.6^{+0.9}_{-1.1}$	$2.2^{+0.3}_{-0.2}$	$-4.1^{+1.2}_{-1.4}$	$1.5^{+0.3}_{-0.3}$
	402080301	$-8.5^{+1.7}_{-2.0}$	$2.3^{+0.5}_{-0.4}$	$-8.5^{+1.7}_{-2.0}$	$2.3^{+0.5}_{-0.4}$	$-14.1^{+3.5}_{\clubsuit}$	$3.6^{+1.1}_{-0.8}$
IC4329A	147440101*	$-0.7^{+0.2}_{-0.2}$	$0.6^{+0.1}_{-0.1}$	$-0.7^{+0.7}_{-0.8}$	$2.0^{+0.2}_{-0.2}$	$-0.7^{+1.0}_{-1.2}$	$1.9^{+0.3}_{-0.2}$
Mrk279	302480401	$-9.5^{+1.5}_{-2.0}$	$2.2^{+0.5}_{-0.3}$	$-10.1^{+1.6}_{-2.2}$	$2.4^{+0.5}_{-0.4}$		
Circinus	111240101	$-4.9^{+0.4}_{-0.5}$	$1.7^{+0.1}_{-0.1}$	$-4.6^{+0.5}_{-0.6}$	$1.6^{+0.2}_{-0.2}$	$-5.2^{+0.6}_{-0.6}$	$1.7^{+0.2}_{-0.2}$
NGC5506	554170101	$-8.1^{+0.5}_{-0.5}$	$2.4^{+0.1}_{-0.1}$	$-6.6^{+0.6}_{-0.8}$	$2.0^{+0.2}_{-0.2}$	$-8.0^{+0.5}_{-0.5}$	$2.3^{+0.1}_{-0.1}$
	0201						
NGC5548	089960301	$-7.8^{+0.6}_{-0.8}$	$2.1^{+0.2}_{-0.2}$	$-7.5^{+0.6}_{-0.8}$	$2.0^{+0.2}_{-0.2}$	$-10.6^{+2.0}_{-2.6}$	$2.6^{+0.6}_{-0.5}$
ESO511-G030	502090201	$-7.3^{+0.8}_{-0.8}$	$1.9^{+0.2}_{-0.2}$	$-7.1^{+0.8}_{-0.8}$	$1.9^{+0.2}_{-0.2}$	$-13.3^{+3.6}_{\clubsuit}$	$3.1^{+1.0}_{-0.8}$
RBS1399	111850201	$-10.5^{+2.4}_{-3.3}$	$2.4^{+0.8}_{-0.6}$	$-24.2^{\clubsuit}$	$5.3^{+4.2}_{-2.0}$	$-5.9^{+1.2}_{-1.5}$	$1.6^{+0.3}_{-0.3}$
	165770201	$-7.7^{+1.6}_{-2.5}$	$1.6^{+0.5}_{-0.3}$	$-9.1^{+2.0}_{-3.3}$	$2.0^{+0.8}_{-0.5}$		
	310190101	$-8.4^{+1.5}_{-2.4}$	$1.9^{+0.6}_{-0.4}$	$-8.6^{+1.6}_{-2.2}$	$2.0^{+0.5}_{-0.4}$	$-9.6^{+3.3}_{\clubsuit}$	$2.3^{+2.0}_{-0.7}$
	0201						
Mrk841	205340201	$-7.3^{+0.9}_{-1.1}$	$2.1^{+0.3}_{-0.2}$	$-7.6^{+1.1}_{-1.3}$	$2.2^{+0.3}_{-0.3}$	$-6.8^{+1.5}_{-1.9}$	$2.0^{+0.4}_{-0.4}$
PKS1549-79	550970101	$-5.1^{+2.0}_{-3.1}$	$1.4^{+0.8}_{-0.4}$			$-6.8^{+2.5}_{-3.3}$	$1.8^{+0.8}_{-0.6}$
PDS456	501580101	$-9.1^{+0.8}_{-0.9}$	$2.5^{+0.2}_{-0.2}$	$-9.0^{+0.8}_{-0.9}$	$2.5^{+0.2}_{-0.2}$	$-8.7^{+1.3}_{-1.6}$	$2.4^{+0.3}_{-0.3}$
	0201						
ESO141-G55	503750101	$-11.4^{+2.4}_{-3.5}$	$2.6^{+0.8}_{-0.6}$	$-12.2^{+2.5}_{-3.4}$	$2.8^{+0.8}_{-0.6}$	$-6.0^{+1.7}_{\clubsuit}$	$1.5^{+3.2}_{-0.4}$
NGC6860	552170301	$-9.8^{+1.0}_{-1.1}$	$2.6^{+0.3}_{-0.2}$	$-8.9^{+0.9}_{-1.0}$	$2.4^{+0.3}_{-0.2}$	$-9.2^{+1.1}_{-1.3}$	$2.5^{+0.3}_{-0.3}$
Mrk509	306090201	$-9.7^{+0.9}_{-1.0}$	$2.3^{+0.2}_{-0.2}$	$-9.4^{+0.9}_{-1.1}$	$2.2^{+0.3}_{-0.2}$	$-9.2^{+1.9}_{-2.4}$	$2.3^{+0.5}_{-0.4}$
	0301						
	0401						
	601390201	$-9.7^{+0.4}_{-0.5}$	$2.3^{+0.1}_{-0.1}$	$-9.7^{+0.5}_{-0.5}$	$2.3^{+0.1}_{-0.1}$	$-10.6^{+0.9}_{-1.0}$	$2.6^{+0.2}_{-0.2}$
	0301						
	0401						
	0501						
	0601						
	0701						
	0801						
	0901						
	1001						
	1101						
IGRJ21277+5656	655450101	$-5.9^{+0.4}_{-0.4}$	$2.0^{+0.1}_{-0.1}$	$-5.8^{+0.4}_{-0.5}$	$1.9^{+0.1}_{-0.1}$	$-5.3^{+0.4}_{-0.4}$	$1.8^{+0.1}_{-0.1}$
PKS2135-14	092850201	$-4.8^{+1.2}_{-1.5}$	$1.3^{+0.4}_{-0.3}$	$-6.2^{+1.6}_{-2.3}$	$1.6^{+0.6}_{-0.4}$	$-1.9^{+1.3}_{-1.3}$	$0.7^{+0.3}_{-0.3}$
PKS2155-304	080940101	$-7.9^{+0.4}_{-0.4}$	$2.2^{+0.1}_{-0.1}$	$-8.0^{+0.4}_{-0.5}$	$2.2^{+0.1}_{-0.1}$	$-8.1^{+0.9}_{-1.1}$	$2.3^{+0.3}_{-0.2}$
	0301						
	124930201	$-8.9^{+0.4}_{-0.5}$	$2.3^{+0.1}_{-0.1}$	$-8.9^{+0.4}_{-0.5}$	$2.3^{+0.1}_{-0.1}$	$-8.5^{+0.8}_{-0.8}$	$2.4^{+0.2}_{-0.2}$
	0301						
	0601						
	158961301	$-8.0^{+0.5}_{-0.5}$	$2.1^{+0.1}_{-0.1}$	$-8.0^{+0.5}_{-0.5}$	$2.1^{+0.1}_{-0.1}$	$-7.3^{+0.9}_{-1.0}$	$2.0^{+0.2}_{-0.2}$
	1401						
	411780201	$-7.6^{+0.3}_{-0.3}$	$2.1^{+0.1}_{-0.1}$	$-7.9^{+0.3}_{-0.3}$	$2.1^{+0.1}_{-0.1}$	$-7.4^{+0.6}_{-0.6}$	$2.1^{+0.2}_{-0.1}$
	0401						
	0501						
	0601						
NGC7172	202860101	$-8.9^{+1.9}_{-2.5}$	$2.4^{+0.6}_{-0.5}$			$-8.5^{+1.8}_{-2.4}$	$2.3^{+0.6}_{-0.4}$
NGC7213	605800301	$-4.8^{+0.9}_{-1.2}$	$1.2^{+0.3}_{-0.2}$	$-5.6^{+1.2}_{-1.6}$	$1.4^{+0.4}_{-0.3}$		
NGC7314	311190101	$-5.0^{+0.4}_{-0.4}$	$1.8^{+0.1}_{-0.1}$	$-4.8^{+0.5}_{-0.5}$	$1.8^{+0.1}_{-0.1}$	$-4.3^{+0.5}_{-0.5}$	$1.6^{+0.1}_{-0.1}$
Ark564	206400101*	$-5.4^{+0.2}_{-0.2}$	$1.9^{+0.1}_{-0.1}$	$-0.7^{+0.4}_{-0.4}$	$1.8^{+0.1}_{-0.1}$	$-5.4^{+1.1}_{-1.6}$	$1.4^{+0.3}_{-0.3}$
MS22549-3712	205390101	$-8.1^{+1.2}_{-1.4}$	$2.4^{+0.4}_{-0.3}$	$-8.8^{+1.2}_{-1.5}$	$2.5^{+0.4}_{-0.3}$	$-2.0^{+0.9}_{-0.9}$	$1.0^{+0.2}_{-0.2}$
NGC7469	207090101	$-9.1^{+0.8}_{-0.8}$	$2.4^{+0.2}_{-0.2}$	$-9.1^{+0.8}_{-0.8}$	$2.4^{+0.2}_{-0.2}$	$-9.3^{+1.3}_{-1.5}$	$2.5^{+0.3}_{-0.3}$
	0201						
NGC7582	204610101	$-2.3^{+1.2}_{-1.2}$	$0.8^{+0.3}_{-0.3}$	$-2.0^{+1.0}_{-1.0}$	$0.8^{+0.3}_{-0.2}$	$-2.2^{+2.2}_{-2.3}$	$0.8^{+0.6}_{-0.5}$

Table 2. Parameters of the fit of to *Model A*.Asterisks mark those observations where the Poisson noise level has been fixed.

Name	ObsID	0.2-10 keV				0.2-2 keV				2-10 keV			
		log(N)	α	log(ν_{br})	log(p)	log(N)	α	log(ν_{br})	log(p)	log(N)	α	log(ν_{br})	log(p)
(1)	(2)	(3)	(4)	(5)	(6)	(7)	(8)	(9)	(10)	(11)	(12)	(13)	(14)
Mrk335	306870101	$-2.3^{+0.2}_{-0.1}$	$3.7^{+0.4}_{-0.4}$	$-3.76^{+0.10}_{-0.12}$	-6.3	$-2.3^{+0.2}_{-0.1}$	$3.6^{+0.4}_{-0.3}$	$-3.80^{+0.10}_{-0.13}$	-5.4	$-2.3^{+0.1}_{-0.1}$	$3.7^{+1.0}_{-0.6}$	$-3.64^{+0.10}_{-0.14}$	-4.0
ESO113-G10	301890101	$-2.2^{+0.2}_{-0.2}$	$3.0^{+0.6}_{-0.4}$	$-3.73^{+0.18}_{-0.26}$	-2.3	$-2.2^{+0.2}_{-0.2}$	$2.9^{+0.6}_{-0.4}$	$-3.75^{+0.19}_{-0.30}$	-2.0	$-2.2^{+0.2}_{-0.1}$	$4.5^{+3.8}_{-1.7}$	$-3.64^{+0.12}_{-0.18}$	-1.8
Mrk586	048740101	$-2.2^{+0.3}_{-0.2}$	$4.2^{+1.3}_{-0.8}$	$-3.92^{+0.15}_{-0.22}$	-1.7	$-2.2^{+0.4}_{-0.2}$	$3.9^{+1.2}_{-0.8}$	$-3.94^{+0.17}_{-0.26}$	-1.5	$-1.9^{+0.2}_{-0.2}$	$10.7^{\clubsuit}$	$-3.78^{+0.11}_{-0.09}$	-2.1
PKS0558-504	555170201	$-1.5^{+0.2}_{-0.2}$	$2.5^{+0.1}_{-0.1}$	$-4.60^{+0.15}_{-0.20}$	-2.5	$-1.5^{+0.2}_{-0.2}$	$2.5^{+0.1}_{-0.1}$	$-4.59^{+0.15}_{-0.20}$	-2.6	$-1.3^{+0.4}_{-0.2}$	$2.4^{+0.2}_{-0.2}$	$-4.78^{+0.26}_{-0.47}$	-1.0
	0301												
	0401												
	0501												
	0601												
1H0707-495	511580101	$-1.4^{+0.1}_{-0.1}$	$2.5^{+0.1}_{-0.1}$	$-3.69^{+0.09}_{-0.10}$	-9.0	$-1.4^{+0.1}_{-0.1}$	$2.5^{+0.1}_{-0.1}$	$-3.69^{+0.09}_{-0.10}$	-9.0	$-1.2^{+0.1}_{-0.1}$	$2.6^{+0.4}_{-0.3}$	$-3.37^{+0.09}_{-0.11}$	-5.2
	0201												
	0301												
	0401												
	653510301	$-1.1^{+0.1}_{-0.1}$	$2.5^{+0.1}_{-0.1}$	$-3.90^{+0.09}_{-0.11}$	-9.0	$-1.2^{+0.1}_{-0.1}$	$2.6^{+0.1}_{-0.1}$	$-3.88^{+0.09}_{-0.10}$	-9.0	$-0.9^{+0.1}_{-0.1}$	$2.2^{+0.2}_{-0.2}$	$-3.50^{+0.13}_{-0.19}$	-4.3

Name	ObsID		0.2-10 keV				0.2-2 keV				2-10 keV		
(1)	(2)	log(N) (3)	α (4)	log(ν_{br}) (5)	log(p) (6)	log(N) (7)	α (8)	log(ν_{br}) (9)	log(p) (10)	log(N) (11)	α (12)	log(ν_{br}) (13)	log(p) (14)
	0401												
	0501												
	0601												
	554710801	$-1.2^{+0.2}_{-0.1}$	$3.0^{+1.2}_{-0.6}$	$-3.46^{+0.19}_{-0.28}$	-2.4	$-1.2^{+0.2}_{-0.1}$	$2.9^{+0.9}_{-0.6}$	$-3.49^{+0.19}_{-0.28}$	-2.4	$-1.1^{+0.1}_{-0.1}$	$7.0^{\clubsuit}_{-4.5}$	$-3.30^{+0.15}_{-0.13}$	-1.1
ESO434-G40	302850201	$-2.7^{+0.3}_{-0.2}$	$3.5^{+0.8}_{-0.6}$	$-4.06^{+0.15}_{-0.23}$	-2.1	$-2.6^{+0.6}_{-0.2}$	$3.0^{+1.2}_{-0.7}$	$-4.27^{+0.26}_{-0.56}$	-0.9	$-2.7^{+0.2}_{-0.2}$	$4.1^{+1.2}_{-0.8}$	$-3.94^{+0.12}_{-0.17}$	-2.9
NGC3227	400270101	$-2.3^{+0.2}_{-0.1}$	$3.4^{+0.5}_{-0.4}$	$-3.64^{+0.12}_{-0.15}$	-4.4	$-2.2^{+0.2}_{-0.1}$	$3.4^{+0.6}_{-0.4}$	$-3.68^{+0.13}_{-0.17}$	-3.9	$-2.5^{+0.2}_{-0.1}$	$3.5^{+1.2}_{-0.8}$	$-3.60^{+0.14}_{-0.21}$	-2.8
KUG1031+398	506440101	$-2.7^{+0.1}_{-0.1}$	$3.3^{+0.9}_{-0.7}$	$-3.44^{+0.11}_{-0.17}$	-2.5	$-2.7^{+0.2}_{-0.1}$	$3.1^{+0.8}_{-0.6}$	$-3.47^{+0.12}_{-0.20}$	-2.2	$-2.1^{+0.2}_{-0.2}$	$-21.4^{\clubsuit}$	$-3.94^{+0.41}_{-0.50}$	-0.7
NGC4051	109141401	$-1.2^{+0.2}_{-0.1}$	$2.5^{+0.2}_{-0.2}$	$-3.56^{+0.17}_{-0.23}$	-3.4	$-1.1^{+0.2}_{-0.2}$	$2.3^{+0.2}_{-0.2}$	$-3.69^{+0.22}_{-0.32}$	-2.4	$-1.3^{+1.3}_{-0.2}$	$1.7^{+0.3}_{-0.2}$	$-3.99^{+0.56}_{-3.27}$	-0.5
	606320101	$-1.3^{+0.1}_{-0.1}$	$2.7^{+0.2}_{-0.1}$	$-3.51^{+0.09}_{-0.11}$	-9.0	$-1.3^{+0.1}_{-0.1}$	$2.6^{+0.2}_{-0.2}$	$-3.55^{+0.10}_{-0.13}$	-7.2	$-1.5^{+0.1}_{-0.1}$	$2.7^{+0.3}_{-0.3}$	$-3.42^{+0.10}_{-0.14}$	-4.9
	0201												
	1601												
	1901												
	2201												
	2301												
Mrk766	109141301	$-1.8^{+0.2}_{-0.1}$	$2.7^{+0.2}_{-0.2}$	$-3.75^{+0.15}_{-0.20}$	-3.8	$-1.8^{+0.2}_{-0.1}$	$2.7^{+0.2}_{-0.2}$	$-3.78^{+0.15}_{-0.21}$	-3.6	$-2.0^{+0.1}_{-0.1}$	$2.8^{+0.8}_{-0.6}$	$-3.27^{+0.13}_{-0.24}$	-2.3
	304030101	$-1.8^{+0.1}_{-0.1}$	$2.9^{+0.2}_{-0.1}$	$-3.69^{+0.08}_{-0.09}$	-9.0	$-1.8^{+0.1}_{-0.1}$	$2.8^{+0.2}_{-0.1}$	$-3.74^{+0.08}_{-0.10}$	-9.0	$-1.6^{\clubsuit}$	$2.0^{\clubsuit}$	$-4.04^{\clubsuit}$	-1.2
	0301												
	0401												
	0501												
	0601												
NGC4395	142830101*	$-1.1^{+0.0}_{-0.1}$	$2.1^{+0.6}_{-0.4}$	$-2.66^{+0.16}_{-0.32}$	-2.2	$2.9^{\clubsuit}_{-4.3}$	$1.8^{+0.2}_{-0.2}$	$-10.20^{\clubsuit}$	0.0	$-1.6^{+3.1}_{-0.9}$	$0.2^{+0.6}_{\clubsuit}$	$-2.68^{+3.64}_{-1.31}$	-0.1
MCG-06-30-015	029740101	$-1.7^{+0.1}_{-0.1}$	$2.8^{+0.1}_{-0.1}$	$-3.79^{+0.09}_{-0.10}$	-9.0	$-1.6^{+0.1}_{-0.1}$	$2.8^{+0.1}_{-0.1}$	$-3.84^{+0.09}_{-0.11}$	-9.0	$-1.8^{+0.1}_{-0.1}$	$2.4^{+0.2}_{-0.2}$	$-3.74^{+0.15}_{-0.21}$	-4.2
	0701												
	0801												
	111570201	$-2.0^{+0.2}_{-0.1}$	$3.4^{+0.5}_{-0.4}$	$-3.50^{+0.12}_{-0.16}$	-4.0	$-2.0^{+0.2}_{-0.1}$	$3.4^{+0.5}_{-0.4}$	$-3.52^{+0.12}_{-0.16}$	-3.9	$-2.1^{+0.2}_{-0.1}$	$2.9^{+0.8}_{-0.5}$	$-3.37^{+0.17}_{-0.27}$	-2.1
Circinus	111240101	$-2.2^{+0.1}_{-0.1}$	$3.2^{+0.8}_{-0.6}$	$-3.39^{+0.11}_{-0.15}$	-3.4	$-2.2^{+0.1}_{-0.1}$	$4.1^{+1.9}_{-1.1}$	$-3.34^{+0.10}_{-0.14}$	-3.0	$-2.1^{+0.6}_{-0.2}$	$2.1^{+0.6}_{-0.4}$	$-3.97^{+0.38}_{-1.21}$	-0.7
NGC5506	554170101	$-2.4^{+0.9}_{-0.1}$	$3.6^{+0.5}_{-1.7}$	$-3.78^{+0.46}_{-0.11}$	-6.4	$-2.7^{+0.1}_{-0.1}$	$9.4^{\clubsuit}_{-3.7}$	$-3.61^{+0.04}_{-0.07}$	-6.1	$-2.4^{+0.1}_{-0.1}$	$3.6^{+0.5}_{-0.4}$	$-3.78^{+0.09}_{-0.11}$	-6.2
	0201												
NGC6860	552170301	$-2.7^{+0.2}_{-0.2}$	$4.6^{+1.6}_{-1.0}$	$-4.03^{+0.11}_{-0.16}$	-3.0	$-2.6^{+0.3}_{-0.2}$	$3.6^{+0.9}_{-0.6}$	$-4.09^{+0.15}_{-0.23}$	-2.1	$-2.8^{+0.2}_{-0.1}$	$10.9^{\clubsuit}$	$-3.87^{+0.04}_{-0.04}$	-3.9
Ark564	206400101	$-1.9^{+0.2}_{-0.1}$	$2.5^{+0.3}_{-0.3}$	$-3.46^{+0.18}_{-0.26}$	-3.0	$-1.9^{+0.2}_{-0.1}$	$2.6^{+0.3}_{-0.3}$	$-3.47^{+0.17}_{-0.25}$	-3.2	$-1.8^{+0.2}_{-0.1}$	$2.2^{\clubsuit}_{-0.6}$	$-3.15^{+0.20}_{-0.65}$	-0.9
MS22549-3712	205390101	$-2.3^{+0.2}_{-0.1}$	$30.9^{\clubsuit}$	$-3.76^{+0.05}_{-0.04}$	-2.2	$-2.2^{+0.3}_{-0.2}$	$8.0^{\clubsuit}_{-4.1}$	$-3.84^{+0.08}_{-0.23}$	-2.1	$-2.0^{+0.1}_{-0.1}$	$25.5^{\clubsuit}$	$-3.00^{+0.19}_{-0.10}$	-0.5

Table 3. Parameters of the PSD fits to *Model B*. Asterisks mark those observations where the Poisson noise level has been fixed.

			Breaks reported in this study							
Name (1)	Ref. (2)	Type (3)	Satellite (4)	Band (5)	log(M_{BH}) (6)	L_{bol} (7)	FWHM(Hβ) (km/s) (8)	α (9)	log(ν_{br}) (10)	$\nu_{br} \times P(\nu_{br})$ ($\times 10^{-3}$) (11)
Mrk335	1	NLSY1	XMM	0.2-10	7.34(1)	44.69(1)	1629	$3.73^{+0.15}_{-0.15}$	$-3.76^{+0.11}_{-0.11}$	2.2 ± 0.3
ESO113-G10	1	S1	XMM	0.2-10		44.17(7)		$2.98^{+0.22}_{-0.22}$	$-3.73^{+0.22}_{-0.22}$	2.9 ± 0.5
PKS0558-504	1	NLSY1	XMM	0.2-10	8.48(12)	46.74(6)	1250*	$2.52^{+0.19}_{-0.19}$	$-4.60^{+0.18}_{-0.18}$	16.6 ± 3.1
1H0707-495	1	NLSY1	XMM	0.2-10	6.37(2)	44.43(2)	935	$2.50^{+0.25}_{-0.25}$	$-3.82^{+0.07}_{-0.07}$	24.2 ± 1.4
ESO434-G40	1	S1	XMM	0.2-10	6.30(3)	44.30(3)	2490*	$3.52^{+0.38}_{-0.38}$	$-4.06^{+0.19}_{-0.19}$	1.0 ± 0.2
NGC3227	1	S1	XMM	0.2-10	6.88(4)	43.86(1)	4920	$3.44^{+0.20}_{-0.20}$	$-3.64^{+0.13}_{-0.13}$	2.2 ± 0.3
KUG1031+398	1	NLSY1	XMM	0.2-10	6.60(5)	44.82(4)	1500	$3.26^{+0.09}_{-0.09}$	$-3.44^{+0.14}_{-0.14}$	1.1 ± 0.1
NGC4051	1	NLSY1	XMM	0.2-10	6.13(4)	43.56(1)	1120	$2.63^{+0.38}_{-0.38}$	$-3.52^{+0.09}_{-0.09}$	25.3 ± 1.9
Mrk766	1	NLSY1	XMM	0.2-10	6.57(6)	44.08(5)	1630	$2.79^{+0.58}_{-0.58}$	$-3.70^{+0.08}_{-0.08}$	7.3 ± 0.5
NGC4395	1	S1	XMM	0.2-10	5.55(7)	41.37(5)	1500	$2.13^{+0.22}_{-0.22}$	$-2.66^{+0.24}_{-0.24}$	37.9 ± 1.7
MCG-06-30-015	1	NLSY1	XMM	0.2-10	6.71(8)	43.85(5)	1700	$2.83^{+0.28}_{-0.28}$	$-3.75^{+0.08}_{-0.08}$	6.9 ± 0.6
Circinus	1	S2	XMM	0.2-10	6.23(14)	43.60(8)	1925	$3.23^{+0.12}_{-0.12}$	$-3.39^{+0.13}_{-0.13}$	3.3 ± 0.4
NGC5506	1	NLSY1	XMM	0.2-10	7.45(9)	44.00(5)	1800*	$3.60^{+0.27}_{-0.27}$	$-3.78^{+0.29}_{-0.29}$	1.9 ± 1.0
NGC6860	1	S1	XMM	0.2-10	7.59(13)	44.53(7)	3900	$4.56^{+0.22}_{-0.22}$	$-4.03^{+0.13}_{-0.13}$	1.0 ± 0.2
Ark564	1	NLSY1	XMM	0.2-10	6.90(9)	44.90(5)	865	$2.51^{+0.11}_{-0.11}$	$-3.46^{+0.22}_{-0.22}$	6.3 ± 1.0

Name (1)	Ref. (2)	Type (3)	Satellite (4)	Band (5)	log(M_{BH}) (6)	L_{bol} (7)	FWHM(Hβ) (km/s) (8)	α (9)	log(ν_{br}) (10)
Mrk 335	2	NLSY1	XMM	0.2-10	7.34(1)	44.69(1)	1629	$3.80^{+1.50}_{-1.50}$	$-3.77^{+0.18}_{-0.53}$
NGC 3227	3	S1	RXTE	2-10	6.88(4)	43.86(1)	4920	>1.90	$-4.59^{+0.36}_{-0.58}$
KUG 1031+398	4	NLSY1	XMM	0.2-10	6.60(5)	44.82(4)	1500	$3.40^{+1.80}_{-1.20}$	$-3.37^{+0.18}_{-0.33}$
NGC 3516	5	S1	RXTE	2-10	7.50(4)	44.29(1)	3350	$2.00^{+0.55}_{-0.25}$	$-5.70^{+0.40}_{-0.30}$
NGC 3783	5,6,7	S1	RXTE	2-10	7.47(10)	44.41(1)	3570	$1.90^{+0.15}_{-0.30}$	$-5.20^{+0.40}_{-0.20}$
NGC 4051	8,9,10	NLSY1	RXTE/XMM	2-10	6.23(4)	43.56(1)	1120	$2.03^{+0.40}_{-0.70}$	$-3.08^{+0.52}_{-1.44}$
NGC 4151	5	S1	RXTE	2-10	7.12(10)	43.73(1)	5000	$2.10^{+1.90}_{-0.25}$	$-5.90^{+0.40}_{-0.70}$
Mrk 766	11,12	NLSY1	XMM	0.2-10	6.57(6)	44.08(5)	1630	$2.80^{+0.20}_{-0.40}$	$-3.30^{+0.08}_{-0.40}$
	11,12		XMM	0.2-0.7				$2.60^{+0.40}_{-0.40}$	$-3.52^{+0.30}_{-0.48}$
	11,12		XMM	0.7-2				$2.70^{+0.50}_{-0.50}$	$-3.30^{+0.20}_{-0.40}$
	11,12		XMM	2-10				$2.30^{+0.40}_{-0.40}$	$-3.30^{+0.20}_{-0.40}$
NGC 4395	13	S1	ASCA	1.2-10	4.70(7)	41.37(5)	1500	$1.78^{+0.19}_{-0.19}$	$-3.49^{+0.30}_{-0.30}$
	14	S1	XMM	2-10				$2.24^{+0.36}_{-0.40}$	$-2.90^{+0.38}_{-0.39}$
Fairall 9	5	S1	RXTE	2-10	8.41(10)	45.23(1)	6270	$2.20^{+0.65}_{-0.20}$	$-6.39^{+0.20}_{-0.40}$
MCG-06-30-015	15	NLSY1	XMM	0.2-10	6.71(8)	43.85(5)	1700	$2.50^{+0.15}_{-0.15}$	$-3.00^{+0.30}_{-0.22}$
	15		XMM	0.2-0.7				$2.55^{+0.20}_{-0.20}$	$-2.89^{+0.34}_{-0.21}$
	15		XMM	0.7-2				$2.30^{+0.15}_{-0.15}$	$-3.10^{+0.30}_{-0.20}$
	15		XMM	2-10				$2.10^{+0.15}_{-0.15}$	$-3.00^{+0.30}_{-0.40}$
	16		RXTE	2-10				$2.00^{+0.30}_{-0.30}$	$-4.29^{+0.30}_{-0.60}$
IC 4329A	17	S1	RXTE/XMM	3-10	8.34(11)	45.52(2)	5960	$2.30^{+0.80}_{-0.40}$	$-5.60^{+0.30}_{-0.49}$
NGC 5506	3	NLSY1	RXTE	2-10	7.45(9)	44.00(5)	1800*	>1.80	$-4.85^{+0.87}_{-0.33}$
NGC 5548	5	S1	RXTE	2-10	7.64(4)	44.83(1)	5800	$2.05^{+0.50}_{-0.65}$	$-6.22^{+0.60}_{-0.70}$
Ark 564	5,18	NLSY1	RXTE	2-10	6.90(9)	44.90(5)	865	$1.20^{+0.25}_{-0.35}$	$-5.80^{+0.60}_{-0.40}$
	19		ASCA	0.7-5				$1.90^{+0.17}_{-0.14}$	$-2.64^{+0.10}_{-0.13}$
	19		ASCA	0.7-2				$1.98^{+0.24}_{-0.20}$	$-2.58^{+0.09}_{-0.11}$
	19		ASCA	2-5				$1.87^{+0.34}_{-0.32}$	$-2.77^{+0.13}_{-0.33}$
PKS 0558-504	20	NLSY1	XMM/RXTE	2-10	8.48(12)	46.74(6)	1250*	$2.21^{+0.24}_{-0.20}$	$-5.17^{+0.22}_{-0.25}$
NGC 7469	21	S1	XMM/RXTE	2-10	7.39(10)	44.56(1)	2650	$1.80^{+0.40}_{-0.40}$	$-6.00^{+0.50}_{-0.40}$

Table 4. Compilation of frequency breaks reported here and in the literature. Note that here we refer to 'S1' to all the AGN with detected broad emission lines. FWHM of Paβ is given (instead of Hβ) for sources marked with asterisks. The references for the PSD fits are: 1. This work, 2. Arévalo et al. (2008), 3. Uttley & McHardy (2005), 4. Vaughan (2010), 5. Markowitz et al. (2003), 6. Arévalo et al. (2009), 7. Summons et al. (2007), 8. McHardy et al. (2004), 9. Papadakis (2004), 10. Vaughan et al. (2011), 11. Vaughan & Fabian (2003), 12. Markowitz et al. (2007), 13. Shih et al. (2003), 14. Vaughan et al. (2005), 15. Vaughan et al. (2003B), 16. McHardy et al. (2005), 17. Markowitz (2009), 18. Papadakis et al. (2002), 19. McHardy et al. (2007), 20. Papadakis et al. (2010), and 21. Markowitz (2010). The references for the bolometric luminosity are: 1. Woo & Urry (2002), 2. Zhou & Wang (2005), 3. Beckmann et al. (2003), 4. Hao et al. (2005), 5. Meyer-Hofmeister & Meyer (2011), 6. Gliozzi et al. (2010), 7. Ponti et al. (2011), and 8. Greenhill et al. (2003). The reserences for the black hole masses are: 1. Grier et al. (2012), 2. Zhou & Wang (2005), 3. Beckmann et al. (2008), 4. Denney et al. (2009), 5. Zhou & Zhao (2010), 6. Botte et al. (2005), 7. Vaughan et al. (2005), 8. McHardy et al. (2005), 9. Sobolewska & Papadakis (2009), 10. Peterson et al. (2004), 11. Markowitz (2009), 12. Gliozzi et al. (2010), 13. Ponti et al. (2011), and 14. Greenhill et al. (2003) .

Appendix A: PSD breaks/bends in the literature

Here we give a short summary of previously reported PSD frequency bends/breaks together and a comparison with our results. Table 4 shows the parameter values discussed here. It should be noted that the *XMM-Newton* data discussed in the present paper are sensitive to bends only in the frequency range from $\gtrsim 10^{-4}$ to ~few$\times 10^{-3}$.

• *Mrk 335*: The 0.2-10 keV band PSD of Mrk 335 was reported by Arévalo et al. (2008) using the same data-set used here. Our results are consistent with theirs.

• *NGC 3227*: Uttley & McHardy (2005) analyzed the 2-10 keV band PSD of NGC 3227 using *RXTE* data and reported a break at 2.6×10^{-5} Hz, a factor ~ 9 lower than our result. Kelly et al. (2011) analysed the *RXTE* and *XMM-Newton* data using a different method for power spectrum estimation, and obtained a bend frequency of $\sim 3.7 \times 10^{-5}$ Hz. Some of the discrepancy between these results and ours may be due to the different energy bands and responses used in the different the analyses, i.e. 2–10 keV *RXTE* data used by Uttley & McHardy (2005) compared to 0.2–10 keV *XMM-Newton* data used here, although it seems unlikely this can account for all the difference.

• *KUG 1031+398*: V10 presented an analysis of the KUG 1031+398 data using essentially the same method as in the present analysis. The two sets of results are fully consistent with each other.

• *NGC 3516*: Markowitz et al. (2003) reported the 2-10 keV PSD of NGC 3516 using *RXTE* data. They found a high-frequency break at $\log(\nu_{\rm b}) = -5.7 \pm 0.4$ (slopes of 1 and 2 below and above the frequency break, respectively). These are outside the frequency range available to the *XMM-Newton* data. As expected we find no strong evidence for a bend within the frequency bandpass considered here, and the Model A slope is consistent with the high frequency slope of Markowitz et al. (2003).

• *NGC 3783*: The power spectrum of this objects has been discussed by Markowitz et al. (2003), Markowitz (2005), Summons et al. (2007), Arévalo et al. (2009) and Kelly et al. (2011) using combinations of *RXTE* and *XMM-Newton* data. These papers report a single bend in the PSD at $\sim 6.2 \times 10^{-6}$Hz, outside the frequency bandpass available to the *XMM-Newton* data. The power spectral slopes reported here are slightly flatter than those reported by Markowitz (2005).

• *NGC 4051*: The PSD of NGC 4051 has discussed by McHardy et al. (2004), Miller et al. (2010) and Vaughan et al. (2011). McHardy et al. (2004) used *RXTE* and *XMM-Newton* data and found a frequency bend at $\log(\nu_{\rm b}) \sim -3.1$, albeit with a large uncertainty. Vaughan et al. (2011) analysed a series of *XMM-Newton* observations, finding broadly similar results but a slightly lower bend frequency ($\log(\nu_b) \sim -3.7$). Here we report a PSD bend at $\log(\nu_{\rm b}) \sim -3.5$, consistent with those reported by with other analyses.

• *NGC 4151*: Markowitz et al. (2003) discussed the 2-10 keV PSD of NGC 4151 using *RXTE* data, and reported a break frequency (using a broken power law model) of $\sim 10^{-6}$ Hz, outside of the frequency bandpass available to the *XMM-Newton* data. The single power-law model (Model A) applied to the *XMM-Newton* data gave a best-fitting slope (2.1) identical to the high frequency slope reported by Markowitz et al. (2003).

• *Mrk 766*: The PSD of Mrk 766 was studied by Vaughan & Fabian (2003), Markowitz et al. (2007) and Kelly et al. (2011). The main parameters (bend frequency and high frequency slope) are broadly compatible with our findings. The bend frequency reported by Markowitz et al. (2007) is slightly higher, but we assumed a low frequency slope of 1 whereas they fitted for this parameter and found a slightly steeper slope.

• *NGC 4395*: Vaughan et al. (2005) report on the PSD using *XMM-Newton* data, and their results are completely consistent with those presented here (their fitting method differs from that used presently). Shih et al. (2003) previously used *ASCA* data to study the PSD of NGC 4395, finding a PSD break at $\log(\nu_b) = -3.5$ (with slopes of $\alpha \sim 1$ and $\alpha \sim 1.8$ at low and high frequencies, respectively). However, the PSD reported by Shih et al. (2003) lacked data in the frequency range $\log(\nu) = [-4, -3.4]$, which hampered accurate estimation of the frequency break.

• *Fairall 9*: Markowitz et al. (2003) and Kelly et al. (2011) discuss the PSD of this source using *RXTE* data. The former paper reports an upper limit on the bend frequency of $\log(\nu_b) \sim -6.4$, and the latter paper gives an estimate of $\log(\nu_b) \approx -5.6$, outside of the frequency bandpass available to the *XMM-Newton* data; as expected given these results we find no strong evidence for a bend in the present analysis. The single power-law fit (i.e. Model A) shows a slope consistent with the previous high frequency slope estimates.

• *MCG–06–30–15*: Vaughan et al. (2003B) and McHardy et al. (2005) have reported on the PSD of this source. In the present paper we report and bend frequency higher than that reported by Vaughan et al. (2003B). However, they used a sharply broken power law while here we use a bending power law model, which means the frequency parameter is not strictly the same. McHardy et al. (2005) analysed together the *RXTE* and *XMM-Newton* data and found a good fit using the bending power law model. Their estimated bend frequency is a factor ≈ 3 lower than that reported in the present paper. This may in part be due to the use of different energy bands between the analyses (e.g. 4–10 keV for *RXTE* and 0.2–10 keV *XMM-Newton*).

• *IC 4329A*: Markowitz (2009) reported the 3-10 keV band PSD. They fitted the PSD to a broken power law with a break at $\log(\nu_{\rm b}) \sim -5.6$, outside of the frequency bandpass avilable to the *XMM-Newton* data. They report a high frequency slope $\alpha = 2.3^{+0.8}_{-0.4}$ consistent with the slope using with Model A in the present study.

• *NGC 5506*: Uttley & McHardy (2005) and Kelly et al. (2011) reported on the PSD of NGC 5506 using *RXTE* data. The PSD bend frequency estimated in the present analysis is a factor ≈ 3 higher. This may in part be due to the use of different energy bands between the analyses (e.g. 2–10 keV for *RXTE* and 0.2–10 keV *XMM-Newton*).

• *NGC 5548*: Markowitz et al. (2003) and Kelly et al. (2011) report on the PSD of NGC 5548. They found a break/bend frequency at $\log(\nu_b) \sim -6.1$, far outside the the frequency bandpass avilable to the *XMM-Newton* data; as expected given these results we find no strong evidence for a bend in the present analysis. The single power-law fit (i.e. Model A) shows a slope consistent with the previous high frequency slope estimates.

• *Ark 564*: The PSD of this source has been discussed by Pounds et al. (2001) and Markowitz et al. (2003) using *RXTE* data, Papadakis et al. (2002) using *ASCA* data, and McHardy et al. (2007) and Kelly et al. (2011) using combinations of these datasets. The bend frequency estimate reported in the present paper is a factor ~ 6 lower than that reported by McHardy et al. (2007), but consistent with that from Kelly et al. (2011). However, as discussed by McHardy et al. (2007) the PSD of this source may be more complicated than the simple bending power law model assumes.

- *PKS 0558-504*: Papadakis et al. (2010) combined *XMM-Newton* and *RXTE* data to estimate a PSD bend frequency of $\log(\nu_b) \approx -5.2$, outside the the frequency bandpass avilable to the *XMM-Newton* data. The apparent detection of a PSD bend, as reported in table 3 is therefore quite unexpected. However, Papadakis et al. (2010) found evidence for a bump (perhaps a broad QPO) in the PSD at frequencies consistent with our bend. Thus, our bend detection is plausibly a misidentification caused by the more complicated PSD shape.
- *NGC 7469*: The 2–10 keV PSD of NGC 7479 was discussed by Markowitz (2010) using *RXTE* and *XMM-Newton* data. The found a bend outside the frequency bandpass available to the *XMM-Newton* data. As expected based on this, we find no evidence for a bend using the *XMM-Newton* data alone. The high frequency slope reported by Markowitz (2010) is consistent with our slope using the single power-law model ($\alpha = 1.8 \pm 0.2$).

Appendix B: Catalogue of PSDs

(online material)